17. Schwarze SR, Ho A, Vocero-Akbani A, Dowdy SF (1999) In vivo protein transduction: delivery of a biologically active protein into the mouse. Science 285: 1569–1572.
18. Yuan F, Salehi HA, Boucher Y, Vasthare US, Tuma RF, et al. (1994) Vascular permeability and microcirculation of gliomas and mammary carcinomas transplanted in rat and mouse cranial windows. Cancer Res 54: 4564–4568.
19. Shah ZA, Namiranian K, Klaus J, Kibler K, Doré S (2006) Use of an optimized transient occlusion of the middle cerebral artery protocol for the mouse stroke model. J Stroke Cerebrovasc Dis 15: 133–138.
20. Chan DA, Sutphin PD, Yen SE, Giaccia AJ (2005) Coordinate regulation of the oxygen-dependent degradation domains of hypoxia-inducible factor 1 alpha. Mol Cell Biol 25: 6415–6426.
21. Hase Y, Okamoto Y, Fujita Y, Kitamura A, Ito H, Maki T, et al. (2012) Cilostazol, a phosphodiesterase inhibitor, prevents no-reflow and hemorrhage in mice with focal cerebral ischemia. Exp Neurol 233: 523–533.
22. Cao G, Pei W, Ge H, Liang Q, Luo Y, et al. (2002) In vivo delivery of a Bcl-xL fusion protein containing the TAT protein transduction domain protects against ischemic brain injury and neuronal apoptosis. J Neurosci 22: 5423–5431.
23. Kilic E, Dietz GP, Hermann DM, Bahr M (2002) Intravenous TAT–Bcl-Xl is protective after middle cerebral artery occlusion in mice. Ann Neurol 52: 617–622.
24. Kilic U, Kilic E, Dietz GP, Bahr M (2003) Intravenous TAT–GDNF is protective after focal cerebral ischemia in mice. Stroke 34: 1304–1310.
25. Kim DW, Eum WS, Jang SH, Kim SY, Choi HS, et al. (2005) Transduced TAT–SOD fusion protein protects against ischemic brain injury. Mol Cells 19: 88–96.
26. Fisher M, Bastan B (2008) Treating acute ischemic stroke. Curr Opin Drug Discov Devel 11: 626–632.
27. Savitz SI, Fisher M (2007) Future of neuroprotection for acute stroke: in the aftermath of the SAINT trials. Ann Neurol 61: 396–402.
28. Labiche LA, Grotta JC (2004) Clinical trials for cytoprotection in stroke. NeuroRx 1: 46–70.
29. Schlaug G, Benfield A, Baird AE, Siewert B, Lövblad KO, et al. (1999) The ischemic penumbra: operationally defined by diffusion perfusion MRI. Neurology 53: 1528–1537.
30. Kucinski T, Naumann D, Knab R, Schoder V, Wegener S, et al. (2005) Tissue at risk is overestimated in perfusion-weighted imaging: MR imaging in acute stroke patients without vessel recanalization. Am J Neuroradiol 26: 815–819.
31. Nedergaard M (1987) Neuronal injury in the infarct border: a neuropathological study in the rat. Acta Neuropathol 73: 267–274.
32. Kinouchi H, Sharp FR, Koistinaho J, Hicks K, Kamii H, et al. (1993) Induction of heat shock HSP70 mRNA and HSP70 kDa protein in neurons in the 'penumbra' following focal cerebral ischemia in the rat. Brain Res 619: 334–338.
33. Wang GL, Semenza GL (1995) Purification and characterization of hypoxia-inducible factor 1. J Biol Chem 270: 1230–1237.
34. Koistinaho J, Pasonen S, Yrjanheikki J, Chan PH (1999) Spreading depression-induced gene expression is regulated by plasma glucose. Stroke 30: 114–119.
35. Gonzalez RG (2006) Imaging-guided acute ischemic stroke therapy: From "time Is brain" to "physiology is brain". Am J Neuroradiol 27: 728–735.

ORIGINAL RESEARCH

Y. Otsuka
H. Yamauchi
N. Sawamoto
K. Iseki
H. Tomimoto
H. Fukuyama

Diffuse Tract Damage in the Hemispheric Deep White Matter May Correlate with Global Cognitive Impairment and Callosal Atrophy in Patients with Extensive Leukoaraiosis

BACKGROUND AND PURPOSE: Patients with extensive leukoaraiosis are at high risk for vascular dementia. However, these patients exhibit variable severity of global cognitive impairment correlating with callosal atrophy. We hypothesized that callosal atrophy may reflect the severity of HDWM tract damage, which may explain global cognitive impairment. The purpose of this study was to evaluate HDWM tract damage by DTI and to investigate whether HDWM tract damage is associated with callosal atrophy and global cognitive impairment, in patients with extensive leukoaraiosis.

MATERIALS AND METHODS: Twenty-four consecutive outpatients with extensive leukoaraiosis were enrolled prospectively. The patients underwent cognitive evaluation and 3T MR imaging. The intercorrelation between cognitive score, DA of the HDWM, callosal DA, and callosal volume was analyzed statistically. The correlation of the cognitive score with DA of the HDWM and the corpus callosum was also evaluated by voxel-based analyses by using TBSS.

RESULTS: The patients' MMSE scores varied from 10 to 30 (mean, 25.1 ± 6.0). Reduced DA of the HDWM, reduced callosal DA, and callosal atrophy intercorrelated significantly. All of these parameters showed a significant correlation with global cognitive impairment. TBSS analyses showed a significant correlation between MMSE score decline and reduced DA in the diffuse HDWM and the corpus callosum.

CONCLUSIONS: In patients with extensive leukoaraiosis, atrophy and reduced DA of the corpus callosum may indicate diffuse HDWM tract damage, which may explain global cognitive impairment and development of vascular dementia.

ABBREVIATIONS: BET = Brain Extraction Tool; DA = diffusion anisotropy; FA = fractional anisotropy; FAB = Frontal Assessment Battery; FMRIB = Functional MR Imaging of the Brain; FWE = family-wise error; HDWM = hemispheric deep white matter; MD = mean diffusivity; MMSE = Mini-Mental State Examination; MNI = Montreal Neurological Institute; NAWM = normal-appearing white matter; TBSS = Tract-based Spatial Statistics; VFT = Verbal Fluency Task; WML = white matter high-intensity lesion; WMSR = *Wechsler Memory Scale–Revised*

Cerebral WMLs, termed "leukoaraiosis,"[1] are observed frequently on T2-weighted MR imaging of elderly patients with lacunar infarcts. WMLs may progress with age, and recent population-based studies have confirmed the relationship between the extent of WMLs and cognitive impairment, especially in executive dysfunction.[2,3] Moreover, extensive WMLs are a radiologic hallmark of Binswanger disease, a common cause of vascular dementia in the elderly.[4,5] Patients with extensive WMLs may be at risk of global cognitive impairment and vascular dementia.[6]

However, patients with extensive WMLs show a variable severity of global cognitive impairment, with some patients showing vascular dementia, whereas others have almost normal cognitive function despite extensive WMLs.[7-9] A longitudinal study demonstrated that further global cognitive deterioration occurs with time in patients with extensive WMLs whose cognitive impairment was mild initially.[6] Therefore, understanding the pathophysiology that may cause a variable severity of cognitive impairment in patients with similar extensive WMLs may lead to the development of optimal therapeutic interventions preventing vascular dementia.

Previous studies have shown that atrophy of the corpus callosum is associated significantly with global cognitive impairment in patients with extensive WMLs.[8,9] The corpus callosum consists of interhemispheric corticocortical connecting fibers, and most of the fibers traverse the HDWM while approaching the contralateral hemisphere.[9] In extensive leukoaraiosis, ischemic insult to the HDWM may affect all of the component fiber tracts, irrespective of their fiber directions.[10] Thus, such ischemic insult may affect callosal fiber tracts in the HDWM where they are passing. Therefore, we hypothesized that diffuse small-vessel ischemia may involve the callosal fiber tracts at the HDWM, in parallel with other HDWM fiber tracts. This ischemic fiber tract damage may cause callosal fiber damage and atrophy and may result in global disconnections among cortical and subcortical networks, leading to global cognitive impairment and vascular dementia. In other words, callosal atrophy may indicate HDWM tract damage and global cognitive impairment in patients with extensive WMLs.

DTI measures the diffusion of water molecules within the

Received May 21, 2011; accepted after revision July 25.

From the Human Brain Research Center (Y.O., H.Y., N.S., K.I., H.F.) and Department of Neurology (H.T.), Kyoto University Graduate School of Medicine, Kyoto, Japan.

Please address correspondence to Yoshinobu Otsuka, MD, Stroke Center, St. Marianna University Toyoko Hospital, 3-435, Kosugi-machi, Nakahara, Kawasaki, 211-0063, Japan; E-mail: otsukay@kuhp.kyoto-u.ac.jp

http://dx.doi.org/10.3174/ajnr.A2853

brain.[11] FA and MD maps are calculated from DTI. Histogram and voxel-based analyses of these maps are useful in evaluating white matter tract damage in patients with extensive WMLs.[12-14] The purpose of this study was to investigate whether HDWM tract damage is associated with global cognitive impairment and callosal atrophy in patients with extensive WMLs and lacunar infarcts, by using histogram and voxel-based analyses of DTI maps.

Materials and Methods

Patient Selection

Twenty-four consecutive patients with lacunar infarcts and extensive WMLs were enrolled prospectively between 2005 and 2007. These patients visited our neurology clinic because of various neurologic symptoms. Inclusion criteria were the following: 1) 60–85 years of age; 2) ≥1 vascular risk factor; 3) irregular and confluent periventricular hyperintensity extending into the deep white matter (Fazekas grade 3) on routine T2-weighted MR imaging that diffusely involved the bilateral hemispheres[15]; and 4) ≥1 lacunar infarct on routine MR imaging. Moreover, 5) patients with dementia (MMSE score, ≤23) were included only if they showed Biswanger dementia-like clinical symptoms, such as dysexecutive syndrome or gait disturbance characterized by start hesitation, short steps and wide stride, slow walking speed, and freezing gait.

The exclusion criteria were the following: 1) 10 history of stroke in the last 4 weeks; 2) history of intracranial hemorrhage; 3) a cortical or callosal infarct or an infarct of >15 mm in diameter in any location on routine MR imaging; 4) strategically located lacunar infarcts possibly causing cognitive impairment such as those in the genu of the internal capsule, thalamus, or caudate nucleus on routine MR imaging[16]; 5) severe dementia with an MMSE score of <10; 6) leukoencephalopathy of nonvascular origin (demyelinating or other); 7) presence of severe systemic or psychiatric illness; or 8) lack of written informed consent from the patients or their closest relatives.

The patients underwent neuropsychological evaluations and 3T MR imaging. Our institutional review board approved the protocol of this study (protocol number E207).

Neuropsychological Evaluations

In addition to screening with MMSE, the patients underwent neuropsychological evaluations including the FAB,[17] VFT,[9] and the Verbal Memory quotient of the WMSR.

MR Imaging Acquisition and DTI Calculations

On the same day as the neuropsychological evaluation, the patient group underwent MR imaging by using a 3T scanner (Trio; Siemens, Erlangen, Germany) equipped with an 8-channel phased array head coil. DTI data were obtained by using a diffusion-weighted single-shot echo-planar imaging sequence (TR = 5200 ms, TE = 77 ms, FOV = 220 mm, matrix size = 128 × 128, voxel size = 1.7 × 1.7 × 3 mm, and 40 axial sections with no intersection gap) with a motion-probing gradient in 12 noncollinear directions (b = 700 s/mm^2). B0 images (b = 0 s/mm^2) were also acquired. These images were processed, and the FA and MD maps were calculated, by using the BET[18] and the Diffusion Toolbox in FMRIB,[19] part of the FMRIB Software Library package, Version 4.0 (FMRIB, Oxford, UK).[20]

3D T1-weighted images were acquired by a magnetization-prepared rapid acquisition gradient echo sequence by using the following parameters: TR = 2000 ms, TE = 4.38 ms, TI = 990 ms, FOV = 240 mm, matrix size = 256 × 224, voxel size = 0.9 × 0.9 × 1 mm, and 208 axial sections. T2-weighted images were acquired by a turbo spin-echo sequence by using the following parameters: TR = 8400 ms, TE = 108 ms, FOV = 220 mm, matrix size = 512 × 416, voxel size = 0.4 × 0.4 × 3 mm, and 40 axial sections with no intersection gap.

Evaluation of DA of the HDWM by Histogram Analyses

Because HDWM DA parameters were needed for statistical analyses, each patient's FA and MD maps were preprocessed to contain only HDWM, subcortical white matter, and cortex, whereas the corpus callosum, ventricle, and other structures were excluded. The calculated histogram parameters from these preprocessed DTI maps were assumed to represent mainly HDWM DA. In detail, we carefully drew ROIs fitting the CSF space, brain stem and cerebellum, and deep structures, such as basal ganglia and diencephalon, on each axial section of individual B0 images. During processing, some of the capsular structures adjacent to the basal ganglia and diencephalon were included in the ROI, despite careful ROI drawing. We applied these ROIs to the corresponding FA and MD maps to exclude these structures. We also carefully drew ROIs fitting the corpus callosum on each axial section of the individual FA map and applied these ROIs to the FA and MD maps to exclude the corpus callosum. Next, the upper 25th percentile value of each patient's FA and MD histograms (FA25 and MD25) and the mean and median values of the FA and MD histograms were calculated.[12] The FA value was assumed to be between 0 and 1, and the MD value was assumed to be between 0 and 500 × 10^{-3} mm^2/s.

Evaluation of Callosal Volume and Callosal DA

We applied the BET application to each patient's 3D T1-weighted image so that extradural voxels were excluded. This image was normalized into 1 × 1 × 1 mm^3 MNI 152 space by linear registration by using the Linear Image Registration Tool of FMRIB.[21] The normalized T1 volume image was segmented into white and gray matter or CSF space; thus, only the white matter was extracted by using the Automated Segmentation Tool in FMRIB.[22] Next, we extracted a midsagittal volume of 10-mm thickness in the standard space and calculated the number of voxels corresponding to the corpus callosum. Because voxel size was normalized to 1 mm^3, the number of voxels multiplied by the voxel size (1 mm^3) gave the normalized callosal volume of the individual patient.

Callosal DA was evaluated on a sagittal plane to exclude possible partial averaging with CSF space. We carefully drew ROIs fitting the corpus callosum on each sagittal section of individual FA maps. Mean callosal FA and MD were calculated in each patient by applying the ROIs to the corresponding FA and MD map.

Evaluation of WML Volume, Lacunar Infarcts, and White or Gray Matter Volume

We also evaluated WML volume, the number and location of lacunar infarcts, and white and gray matter volume to investigate the correlation between these values and cognitive impairment. For evaluating WML volume, the ROIs fitting the WMLs were carefully drawn on each axial section of individual T2-weighted images. The area covered by the ROIs in every section was calculated, and the calculated area of all the sections was summed. Because the section thickness was 3 mm, individual WML volumes were approximated to the summed area multiplied by the section thickness.

A lacunar infarct was defined as follows: 1) a distinct area 3–15 mm in diameter, 2) located in the upper two-thirds of the lentiform

nuclei, cerebral white matter, or pons (patients with lacunae in the caudate nucleus or thalamus were excluded according to the exclusion criterion 4; 3) T1 low intensity; and 4) marked T2 high intensity accompanied by an ill-defined hyperintensity rim. The number of the lacunar infarcts was counted for each location.

The SIENAX application, part of the FMRIB Software Library Package,[23] was applied to each patient's 3D T1 volume, to estimate the individual white and gray matter volumes normalized for each patient's skull size. A board-certified stroke neurologist (Y.O.) with 18 years' experience in neuroradiology blinded to patients' clinical information performed the image processing described above, including ROI processing of DTI and evaluation of WML volume and lacunae.

Statistical Analyses

The intercorrelation between HDWM DA (FA25, MD25, and mean and median values of FA and MD), callosal DA (mean callosal FA and MD), normalized callosal volumes, and cognitive scores (MMSE, FAB, VFT, and WMSR) was analyzed by using the Spearman rank correlation ($|\rho| \geq 0.40$ and $P < .05$ were considered to be significant). Correlation between HDWM DA, callosal DA, or callosal volume and each cognitive score was also examined by stepwise regression analyses and multiple regression analyses. In the stepwise regression analyses, age, sex, number of lacunar infarcts, WML volume, and gray and white matter volume were used as covariables. The multiple regression analyses were adjusted for age, sex, WML volume, and white matter volume. The absolute value of a standardized regression coefficient of >0.40 and $P < .05$ was considered to be significant. Correlation between cognitive scores and age, number of lacunar infarcts, WML volume, gray matter volume, or white matter volume, as well as correlation between HDWM DA and WML volume, was also examined by using the Spearman rank correlation ($|\rho| \geq 0.40$ and $P < .05$ were significant).

Image processing of the FA and MD images for voxel-based analysis was performed by using TBSS (Version 1.1, FMRIB).[24] TBSS enables investigations of white matter tracts without the limitations caused by alignment inaccuracies and by uncertainty concerning smoothing extent that are typical of other voxel-based methods in DTI map analyses.[24] The usefulness of TBSS for voxel-based analyses of DTI maps has been reported in patients with leukoaraiosis and other disease processes involving white matter.[14,24] First, any patient's FA image was aligned to every other patient's FA image, and the most representative image among all patients' FA images was identified and selected as the target image. Next, this target image was affine-aligned into a $1 \times 1 \times 1$ mm^3 MNI 152 space. Every image was then transformed to match the MNI 152 space by combining the nonlinear registration to the target image and the affine registration from that target to the MNI 152 space. A mean FA image was created and thinned to create a mean FA skeleton image, which represents the centers of all tracts in common among the group. Every patient's aligned FA data were then projected onto this skeleton, and the projected FA data of all patients were used for voxel-based cross-subject statistical analysis. Finally, we carried out voxel-based analysis to investigate where FA and MD values had a significant correlation with the cognitive score, adjusted for WML volume and white matter volume, by using permutation-based inference on cluster size ($t > 2$, FWE-corrected $P < .05$; permutation number, 5000) with the Randomise application.[25]

Results

The age of the patients ranged from 61 to 85 (mean, 74 ± 6) years, and 14 of the 24 patients were men. All patients had a history of hypertension. There were 4 patients with hyperlipidemia and with diabetes mellitus, respectively. The MMSE score ranged from 10 to 30 (mean, 25.1 ± 6.0), and the MMSE score showed a strong correlation with the other 3 test batteries (Spearman ρ values: versus FAB: $\rho = 0.83$, $P < .0001$; versus VFT: $\rho = 0.70$, $P = .001$; versus WMSR: $\rho = 0.78$, $P = .0007$). The number of lacunar infarcts varied from 3 to 16 (mean, 8.5 ± 3.7), and most were located in the lentiform nuclei or cerebral white matter. The number of lacunar infarcts was not significantly correlated with cognitive impairment, regardless of location. Patient age, sex, or gray matter volume did not show a significant correlation with cognitive scores.

The WML volume ranged from 52 to 139 cm^3 (mean, 87 ± 2 cm^3). No patient showed high-intensity lesions in the corpus callosum. The increased WML volume showed a significant correlation with WMSR score decline ($\rho = -0.52$, $P = .024$), whereas there was no significant relationship between the WML volume and the MMSE, FAB, or VFT score. White matter volume showed a significant correlation with the VFT score ($\rho = 0.55$, $P = .01$), whereas there was no significant relationship between white matter volume and other cognitive scores.

The DTI histogram of the HDWM showed that the patients with dementia had decreased voxel counts of high FA value and low MD value, while they had increased voxel counts of low FA value and high MD value compared with the data from the patients without dementia (Fig 1). The FA value had a strong negative correlation with the MD value in the HDWM (FA25 versus MD25, $\rho = -0.83$, $P < .0001$; median FA versus median MD, $\rho = -0.77$, $P = .0002$; and mean FA versus mean MD, $\rho = -0.83$, $P < .0001$) and in the corpus callosum (mean callosal FA versus MD, $\rho = -0.90$, $P < .0001$). Reduced HDWM DA, represented by FA reduction and MD increase, reduced callosal DA, and callosal atrophy, all had a strong correlation with global cognitive impairment (Table 1 and Fig 2). Stepwise regression analyses, including age, sex, number of lacunar infarcts, WML volume, and gray and white matter volume as covariables, produced a model in which only each of HDWM DA, callosal DA, or callosal volume was included. The other covariables did not contribute significantly to the magnitude of the correlations, except for a small contribution of the WML volume or white matter volume to some of the correlations. Multiple regression analyses, including age, sex, WML volume, and white matter volume as covariables, confirmed that reduced HDWM DA, reduced callosal DA, and callosal atrophy were independent predictors of cognitive impairment. The WML volume, white matter volume, or other covariables were not an independent predictor in these models, except for a weak contribution of white matter volume to the correlation between callosal MD and VFT score (Table 2).

Reduced HDWM DA was strongly correlated with reduced callosal DA and callosal atrophy (Table 3). Callosal atrophy showed a strong correlation with reduced callosal DA (callosal volume versus mean callosal FA: $\rho = 0.80$, $P < .005$; versus mean callosal MD: $\rho = -0.73$, $P < .005$). Thus, reduced HDWM DA, reduced callosal DA, and callosal atrophy were strongly intercorrelated, and all had a strong correlation with

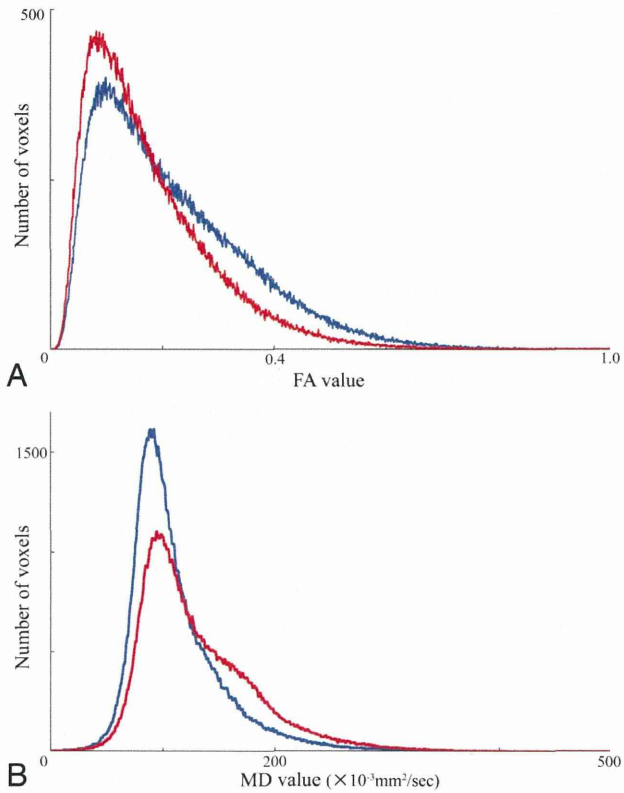

Fig 1. Representative FA (*A*) and MD (*B*) histograms of the HDWM. In both histograms, averaging the histograms of 4 patients with almost normal cognitive function (MMSE 29–30) is represented in blue, whereas averaging the histograms of 4 patients with dementia (MMSE 10–16) is represented in red.

Table 1: Correlation between HDWM DA or callosal parameters and cognitive scores[a]

	MMSE	FAB	VFT	WMSR
HDWM DA				
FA25	0.77[b]	0.76[b]	0.69[b]	0.77[b]
Median FA	0.67[b]	0.73[b]	0.61[c]	0.62[d]
Mean FA	0.74[b]	0.74[b]	0.66[e]	0.73[f]
MD25	−0.75[b]	−0.73[b]	−0.72[b]	−0.84[b]
Median MD	−0.72[b]	−0.71[b]	−0.70[b]	−0.84[b]
Mean MD	−0.74[b]	−0.67[b]	−0.68[f]	−0.85[b]
Callosal mean FA	0.95[b]	0.89[b]	0.80[b]	0.75[b]
Callosal mean MD	−0.90[b]	−0.72[b]	−0.71[b]	−0.85[b]
Callosal volume	0.75[b]	0.83[b]	0.86[b]	0.63[d]

[a] Figures are Spearman ρ values.
[b] Significant after Bonferroni correction for multiple comparisons ($P < .05/36 = .00139$).
[c] $P = .0042$.
[d] $P = .007$.
[e] $P = .0021$.
[f] $P = .0014$.

global cognitive impairment (Fig 3). Only a nonsignificant trend for a weak correlation between WML volume increase and reduced HDWM DA was observed (WML volume versus FA25: $\rho = -0.34$, $P = .10$; versus MD25: $\rho = 0.38$, $P = .07$; versus median FA: $\rho = -0.15$, $P = .48$; versus median MD: $\rho = 0.38$, $P = .07$; versus mean FA: $\rho = -0.31$, $P = .14$; versus mean MD: $\rho = 0.36$, $P = .09$).

Voxel-based analyses with TBSS testing, when adjusted for WML volume and white matter volume, showed that both FA reduction and MD increase had a significant correlation with MMSE score deterioration in both the diffuse HDWM and the corpus callosum (Fig 4).

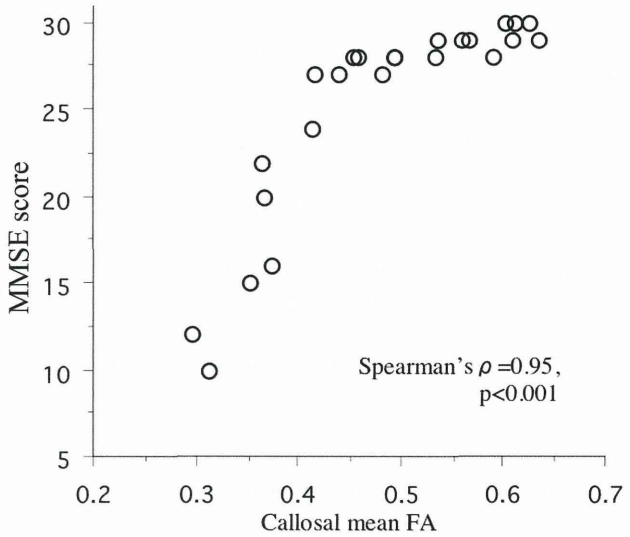

Fig 2. Scatterplot of callosal mean FA values against MMSE scores in each patient.

Table 2: Correlation between HDWM DA or callosal parameters and cognitive scores evaluated with multiple regression analyses[a]

	MMSE	FAB	VFT	WMSR
HDWM DA				
FA25	0.76[b]	0.79[b]	0.64[c]	0.72[b]
Mean FA	0.71[b]	0.73[b]	0.56[d]	0.66[c]
MD25	−0.99[b]	−0.89[b]	−0.59[e]	−0.83[b]
Mean MD	−0.91[b]	−0.78[b]	−0.52[f]	−0.86[b]
Callosal mean FA	0.80[b]	0.85[b]	0.70[b]	0.73[g]
Callosal mean MD	−0.74[b]	−0.66[b]	−0.59[g,h]	−0.82[b]
Callosal volume	0.74[b]	0.8[b]	0.72[b]	0.63[f]

[a] Figures are standardized regression coefficients between each of the HDWM DA or callosal parameters and each of the cognitive scores, adjusted for age, sex, WML volume, and white matter volume.
[b] Significant after Bonferroni correction ($P < .05/28 = .0018$).
[c] $P = .002$.
[d] $P = .006$.
[e] $P = .02$.
[f] $P = .03$.
[g] $P = .003$.
[h] White matter volume showed a weak contribution to the correlation between callosal MD and VFT (standard regression coefficient, 0.43; $P = .046$).

Table 3: Correlation between HDWM DA and callosal parameters[a]

HDWM DA	Callosal Mean FA	Callosal Mean MD	Callosal Volume
FA25	0.73[b]	−0.69[b]	0.71[b]
Median FA	0.63[b]	−0.56[c]	0.72[b]
Mean FA	0.70[b]	−0.66[b]	0.70[b]
MD25	−0.71[b]	0.69[b]	−0.83[b]
Median MD	−0.70[b]	0.69[b]	−0.76[b]
Mean MD	−0.68[b]	0.71[b]	−0.74[b]

[a] Figures are Spearman ρ values.
[b] Significant after Bonferroni correction for multiple comparison ($P < .05/18 = .00278$).
[c] $P = .008$.

Discussion

The present study supports our hypothesis that diffuse HDWM tract damage is associated with global cognitive impairment and callosal atrophy in patients with extensive leukoaraiosis. In our patients with extensive WMLs, reduced HDWM DA showed a strong correlation with global cognitive impairment. The correlation was stronger than that of WML volume with cognitive impairment, and multivariate analyses showed that the correlation was not confounded by WML volume or other factors. Therefore, the patients may have vari-

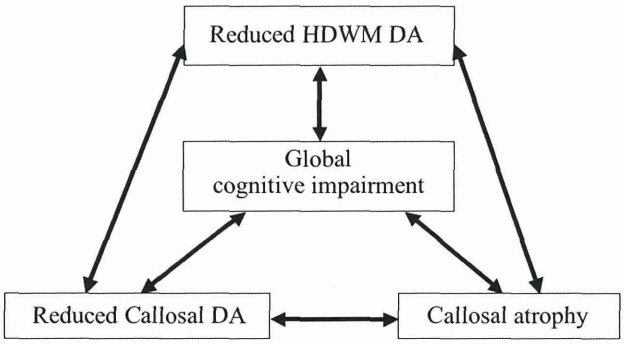

Fig 3. Schematic diagram of the intercorrelation between reduced HDWM DA, reduced callosal DA, callosal atrophy, and cognitive impairment.

able severity of HDWM tract damage that may be detected sensitively by DTI, despite a similar grade of extensive WMLs. Such tract damage may cause global disconnection between cortical and subcortical networks, resulting in global cognitive impairment and vascular dementia.

Moreover, reduced callosal DA and callosal atrophy showed a strong intercorrelation, and both had a strong correlation with reduced HDWM DA. In addition, these callosal parameters also showed a strong correlation with global cognitive impairment that was independent of WML volume, white matter volume, or other covariables. These results support our hypothesis that diffuse ischemic tract damage of the HDWM may cause damage to the passing callosal fiber tracts, resulting in reduced callosal DA and callosal atrophy. These callosal parameters may be sensitive markers of diffuse HDWM tract damage and may be useful for monitoring disease progression and evaluation of treatment efficacy.

Degradation of the microstructural organization in white matter is accompanied by FA reduction and MD increase.[26] There is pathologic evidence that FA and MD correlate with axonal count and the amount of myelin in the white matter.[27] Animal studies have suggested that axonal membranes, rather than the presence of myelin, may contribute primarily to DA.[11] In addition, results from animal studies have indicated that axonal damage is related to reduced diffusibility changes parallel to the primary fiber orientation, while myelin breakdown is related to increased diffusibility perpendicular to the white matter tract.[28] A clinical study in patients with cerebral edema caused by hepatic encephalopathy exhibited no decrease in FA but a significant increase in MD, which was reversible after treatment.[29] Therefore, the combination of FA reduction and MD increase that was observed in the patients may reflect the severity of the white matter tract damage caused by several pathologic processes, including axonal damage, demyelination, and interstitial or extracellular fluid increase in response to chronic small vessel ischemia.

A main limitation of the histogram analyses is the loss of the topographic information. In the present study, the histogram analyses were preceded by segmentation to extract HDWM, subcortical white matter, and cortex data. Graphic representation of the FA histogram in the patients with dementia exhibited the reduction of high DA components corresponding to the deep white matter structure (Fig 1). Therefore, the result of histogram analyses may reflect mainly the severity of HDWM tract damage.

Several recent DTI studies have suggested that NAWM as well as WMLs show reduced DA, which contributed to global cognitive impairment in the patients with WMLs.[3,7,26] Although the histogram approach focusing on NAWM was not performed in the present study because of difficulties in the precise extraction of NAWM in our patients with extensive WMLs, voxel-based analyses showed that the corpus callosum without WMLs and diffuse HDWM had reduced DA, showing significant correlation with global cognitive impairment. Thus, the results of the present study are consistent with those of previous studies in which the white matter tract damage was

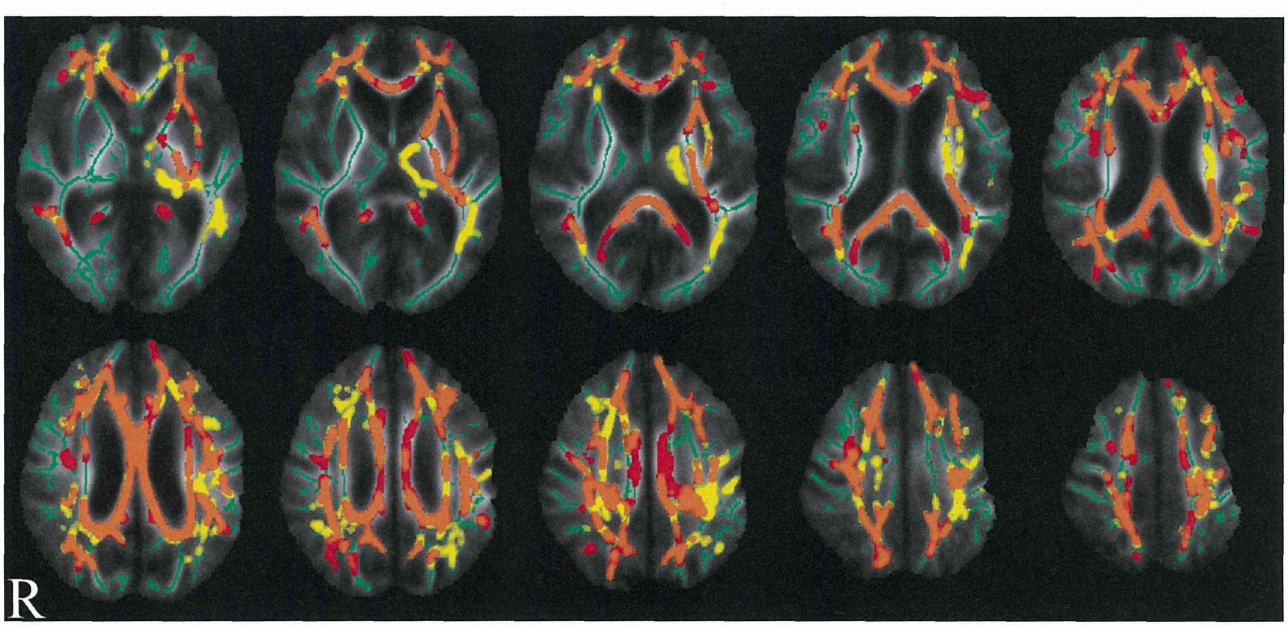

Fig 4. Result of voxel-based analysis of FA and MD maps by using TBSS. Orange shows where both FA reduction and MD increase had significant correlation with the MMSE score decline. Red or yellow shows where FA reduction or MD increase had significant correlation with the MMSE score decline, respectively. All results are adjusted for WML volume and white matter volume. Permutation-based inference on cluster size: $t > 2$, FWE-corrected $P < .05$; permutation number, 5000. Green is the mean FA skeleton, underneath the orange, red, and yellow. In the background is the mean FA image of the 24 patients in the study.

extensive beyond the WMLs. Diffuse HDWM damage may be a summation of damage in the WMLs and NAWM. A method that enables the precise extraction of NAWM from DTI maps of patients with extensive WMLs would clarify the contribution of WMLs versus NAWM to HDWM damage.

Patients with extensive WMLs are associated with a risk of Alzheimer disease, as well as vascular dementia.[30] In the present study, patients with dementia were included only if they had Binswanger dementia-like clinical symptoms. These patients had a vascular risk factor and a history of lacunar infarcts along with extensive WMLs. Moreover, patients with severe dementia of an MMSE <10 were excluded. Thus, in our cohort, the patients with dementia fulfilled the diagnostic criteria of Binswanger disease of Bennett et al.[5] In their series, most of the patients diagnosed pathologically as having Binswanger disease met the criteria compared with only 1.6% of the patients with clinically typical Alzheimer disease.[5] Therefore patients with Alzheimer disease would likely be excluded from our series, though this exclusion was not confirmed pathologically.

In our patients, lacunar infarcts of the lentiform nuclei did not show significant association with cognitive impairment, inconsistent with a previous study that included subjects with various degree of WMLs.[31] We evaluated lacunar infarcts with T1 and T2 high-resolution images. Using high-resolution FLAIR images may allow more precise evaluation of lacunae. However, we excluded lesions <3 mm in diameter or lesions located in the lower one-third of the basal ganglia. A pathologic study has shown that this exclusion may enable differentiation between lacunar infarcts and the perivascular space.[32] Thus, our criteria likely differentiated lacunar infarcts from the perivascular space, though this was not confirmed pathologically. Therefore the inconsistency may possibly result from the small sample size of our study rather than from confusing lacunar infarct with the perivascular space.

We used the MMSE score as a representative cognitive parameter for the voxel-based analyses because of the strong correlation between MMSE and other cognitive batteries. To investigate the pathophysiology causing variable severity of cognitive impairment in patients with similar extensive WMLs, we had to exclude the potential confounding effect of WML extension, as much as possible. Therefore, we recruited only patients with Fazekas grade 3. This criterion may have contributed to our sample characteristics of high cognitive contrast and the strong intercorrelation among cognitive batteries. In the patients with a variable extent of WMLs, executive function may be sensitive to detecting cognitive impairment, as reported in previous population-based studies.[6,7,13]

Our study has several methodologic limitations. First, we used several DTI parameters (eg, FA25 or MD25 and so forth) for the histogram analyses according to a previous study.[12] The peak height of the FA or MD histogram may be more appropriate as a parameter because it is reported to be sensitive to cognitive impairment.[13] Second, we evaluated WMLs with T2 high-resolution images. Using high-resolution FLAIR images may allow more precise evaluation of WMLs. Third, we used several ROIs in the preprocessing of DTI maps. Although these ROIs were carefully drawn, automation of this image processing may improve the reproducibility of our data. Finally, because our study is a single hospital-based cross-sectional study of a small sample size, it is likely that the contrast of WML extension was not sufficient to generate a significant correlation. Population-based multicentered longitudinal and cross-sectional studies recruiting more patients with extensive WMLs and evaluating them with histogram and voxel-based approaches similar to those in our study are warranted to confirm our hypothesis.

Conclusions

In patients with extensive WMLs, reduced HDWM DA, reduced callosal DA, and callosal atrophy were strongly intercorrelated. These parameters showed a strong correlation with global cognitive impairment that was independent from WML extension. Reduced callosal DA and callosal atrophy may represent a surrogate marker of HDWM tract damage, and these callosal parameters as well as DTI parameters of the HDWM may be useful for monitoring disease progression and treatment efficacies.

References

1. Hachinski VC, Potter P, Merskey H. **Leuko-araiosis.** *Arch Neurol* 1987;44:21–23
2. van der Flier W, van Straaten E, Barkhof F, et al, on behalf of the LADIS Study group. **Small vessel disease and general cognitive function in non-disabled elderly: the LADIS Study.** *Stroke* 2005;36:2116–20
3. Schmidt R, Ropele S, Ferro J, et al, on behalf of the LADIS Study group. **Diffusion-weighted imaging and cognition in the leukoaraiosis and disability in the elderly study.** *Stroke* 2010;41:e402–08
4. Roman GC. **Senile dementia of the Binswanger type: a vascular form of dementia in the elderly.** *JAMA* 1987;258:1872–88
5. Bennett DA, Wilson RS, Gilley DW, et al. **Clinical diagnosis of Binswanger's disease.** *J Neurol Neurosurg Psychiatry* 1990;53:961–65
6. Jokinen H, Kalska H, Ylikoski R, et al, on behalf of the LADIS Study group. **Longitudinal cognitive decline in subcortical ischemic vascular disease: the LADIS Study.** *Cerebrovasc Dis* 2009;27:384–91
7. O'Sullivan M, Morris RG, Huckstep B, et al. **Diffusion tensor MRI correlates with executive dysfunction in patients with ischaemic leukoaraiosis.** *J Neurol Neurosurg Psychiatry* 2004;75:441–47
8. Yamauchi H, Fukuyama H, Ogawa M, et al. **Callosal atrophy in patients with lacunar infarction and extensive leukoaraiosis: an indicator of cognitive impairment.** *Stroke* 1994;25:1788–93
9. Yamauchi H, Fukuyama H, Shio H. **Corpus callosum atrophy in patients with leuko-araiosis may indicate global cognitive impairment.** *Stroke* 2000;31:1515–20
10. Yamanouchi H, Sugiura S, Tomonaga M. **Decrease in nerve fiber in cerebral white matter in progressive subcortical vascular encephalopathy of Binswanger type: an electron microscopic study.** *J Neurol* 1989;236:382–87
11. Beaulieu C. **The basis of anisotropic water diffusion in the nervous system: a technical review.** *NMR Biomed.* 2002;15:435–55
12. Della Nave R, Foresti S, Pratesi A, et al. **Whole-brain histogram and voxel-based analyses of diffusion tensor imaging in patients with leukoaraiosis: correlation with motor and cognitive impairment.** *AJNR Am J Neuroradiol* 2007;28:1313–19
13. Nitkunan A, Barrick TR, Charlton RA, et al. **Multimodal MRI in cerebral small vessel disease: its relationship with cognition and sensitivity to change over time.** *Stroke* 2008;39:1999–2005
14. de Laat KF, Tuladhar AM, van Norden AG, et al. **Loss of white matter integrity is associated with gait disorders in cerebral small vessel disease.** *Brain* 2011;134(pt 1):73–83. Epub 2010 Dec 14
15. Fazekas F, Chawluk JB, Alavi A, et al. **MR signal abnormalities at 1.5T in Alzheimer's dementia and normal aging.** *AJR Am J Roentogenol* 1987;149:351–56
16. Tatemichi TK. **Dementia.** In: Bogousslavsky J, Caplan L, eds. *Stroke Syndromes.* New York: Cambridge University Press; 1995, 169–81
17. Dubois B, Slachevsky A, Litvan I, et al. **The FAB: a Frontal Assessment Battery at bedside.** *Neurology* 2000;55:1621–26
18. Smith SM. **Fast robust automated brain extraction.** *Hum Brain Mapping* 2002;17:143–55
19. Behrens TE, Woolrich MW, Jenkinson M, et al. **Characterization and propagation of uncertainty in diffusion-weighted MR imaging.** *Magn Reson Med* 2003;50:1077–88
20. Smith SM, Jenkinson M, Woolrich MW, et al. **Advances in functional and structural MR image analysis and implementation as FSL.** *Neuroimage* 2004;23:208–19

21. Jenkinson M, Smith SM. **A global optimization method for robust affine registration of brain images.** *Med Image Anal* 2001;5:143–56
22. Zhang Y, Brady M, Smith S. **Segmentation of brain MR images through a hidden Markov random field model and the expectation maximization algorithm.** *IEEE Trans Med Imaging* 2001;20:45–57
23. Smith SM, Zhang Y, Jenkinson M, et al. **Accurate, robust and automated longitudinal and cross-sectional brain change analysis.** *Neuroimage* 2002;17:479–89
24. Smith SM, Jenkinson M, Johansen-Berg H, et al. **Tract-based spatial statistics: voxelwise analysis of multi-subject diffusion data.** *Neuroimage* 2006;31:1487–505
25. Nichols TE, Holmes AP. **Nonparametric permutation tests for functional neuroimaging: a primer with examples.** *Hum Brain Mapping* 2001;15:1–25
26. Vernooij MW, Afran Ikram M, Vrooman HA, et al. **White matter microstructural integrity and cognitive function in a general elderly population.** *Arch Gen Psychiatry* 2009;66:545–53
27. Schmierer K, Wheeler-Kingshott CA, Boulby PA, et al. **Diffusion tensor imaging of post mortem multiple sclerosis brain.** *Neuroimage* 2007;35:467–77
28. Song SK, Sun SW, Ju WK, et al. **Diffusion tensor imaging detects and differentiates axon and myelin degeneration in mouse optic nerve after retinal ischemia.** *Neuroimage* 2003;20:1714–22
29. Kale RA, Gupta RK, Saraswat VA, et al. **Demonstration of interstitial cerebral edema with diffusion tensor MR imaging in type C hepatic encephalopathy.** *Hepatology* 2006;43:698–706
30. Debette S, Markus HS. **The clinical importance of white matter hyperintensities on brain magnetic resonance imaging: systematic review and meta-analysis.** *BMJ* 2010;341:c3666
31. Benistry S, Gouw AA, Porcher R, et al, on behalf of the LADIS Study group. **Location of lacunar infarcts correlates with cognition in a sample of non-disabled subjects with age-related white-matter changes: the LADIS Study.** *J Neurol Neurosurg Psychiatry* 2009;80:478–83
32. Bokura H, Kobayashi S, Yamaguchi S. **Distinguishing silent lacunar infarction from enlarged Virchow-Robin spaces: a magnetic resonance imaging and pathological study.** *J Neurol* 1998;245:116–22

Clinical Investigative Study

In vivo Detection of Cortical Microinfarcts on Ultrahigh-Field MRI

Yuichiro Ii, MD, Masayuki Maeda, MD, PhD, Hirotaka Kida, MD, Ko Matsuo, MD, Akihiro Shindo, MD, Akira Taniguchi, MD, Hidekazu Tomimoto, MD, PhD

From the Department of Neurology (YI, KM, AS, AT, HT); Department of Radiology (MM); and Dementia Prevention and Therapeutic (HK), Mie University Graduate School of Medicine, Mie, Japan.

ABSTRACT

BACKGROUND AND PURPOSE

Cortical microinfarcts (CMIs) are detected as small foci restricted to the cerebral cortex in autopsy brains. CMIs are thought to be caused by cerebral amyloid angiopathy (CAA) in the elderly and may be a risk for dementia. We aimed to visualize CMIs, which remain invisible on conventional MRI, using double inversion recovery (DIR) and 3-dimensional fluid attenuated inversion recovery (3D-FLAIR) on 3-Tesla MRI.

METHODS

We prospectively performed DIR and 3D-FLAIR images in 70 subjects with Alzheimer disease (AD; $n = 47$), mild cognitive impairment ($n = 14$), AD with cerebrovascular disease (CVD; $n = 3$), vascular dementia (VaD; $n = 2$), CAA-associated intracerebral hemorrhage (ICH; $n = 2$) and one each of normal pressure hydrocephalus and dementia with Lewy bodies (DLB). Susceptibility-weighted imaging (SWI) was performed to detect cerebral microbleeds (CMBs).

RESULTS

Nine subjects (five of AD and one each of AD with CVD, ICH, VaD, and DLB) had small intracortical high signal lesions on both DIR and 3D-FLAIR images. All the nine subjects accompanied multiple lobar CMBs. These intracortical lesions were located in close proximity to CMBs, and were suggested to be CMIs.

CONCLUSIONS

DIR and 3D-FLAIR images may open a way to visualize CMIs.

Keywords: Alzheimer disease, cortical microinfarcts, MRI, double-inversion recovery, cerebral amyloid angiopathy.

Acceptance: Received September 27, 2011, and in revised form February 21, 2012. Accepted for publication March 14, 2012.

Disclosure: none

Correspondence: Address correspondence to Yuichiro Ii, MD, Department of Neurology, Mie University Graduate School of Medicine, 2–174, Edobashi, Tsu, Mie 514–8507, Japan. E-mail: ii-y@clin.medic.mie-u.ac.jp.

J Neuroimaging 2013;23:28-32.
DOI: 10.1111/j.1552-6569.2012.00722.x

Introduction

Cortical microinfarcts (CMIs) are reported to be an important risk factor for dementia.[1-3] These lesions are frequently detected as small foci restricted to the cerebral cortex in autopsy brains of elderly subjects, and distributed predominantly in the area of predilection for cerebral amyloid angiopathy (CAA) with or without Alzheimer disease (AD) pathology.[1-6] Moreover, CMIs are usually found very close to Aβ-laden small vessels with severe morphological changes,[5] thereby indicating that compromised blood flow or blood–brain barrier (BBB) because of CAA may cause CMIs.

CAA occasionally manifest as cerebral hemorrhage, ischemic stroke, and cognitive decline. Indeed, 78-100% of AD brains exhibit CAA,[7] and in a population-based autopsy study severe CAA was found more frequently (43%) in demented patients compared with nondemented patients (24%).[8] CAA most commonly affects the leptomeningeal arteries, and frequently the intracortical arteries, but rarely involves the medullary arteries in the white matter. Along with the deposition of Aβ, the smooth muscle cells in the media gradually degenerate and may eventually result in lobar cerebral hemorrhages. Small vessels damaged by Aβ deposits become leaky and easy to rupture with migration of hemosiderin-laden macrophages in and around the vessel walls, and these lesions may manifest as cerebral microbleeds (CMBs) on magnetic resonance imaging (MRI).[9] In the past, CAA has been diagnosed postmortem, but recently, gradient echo T2*-weighted imaging and susceptibility-weighted imaging (SWI) on MRI are increasingly recognized as a tool for detecting CMBs in a lobar distribution, being indicative of CAA in elderly subjects.[10,11]

Radiological diagnosis for CAA may be reinforced by detecting CMIs in combination with lobar CMBs, however, CMIs remained invisible on conventional MRI.[12] Recently, double inversion recovery (DIR) has been widely used and commercially installed in 3-Tesla (3T) Phillips MR machine, but not yet in other vendors' 3T machines. However, this sequence will spread in other manufactures in near future. DIR and 3-dimensional fluid attenuated inversion recovery (3D-FLAIR) sequences have become available to detect intracortical small lesions in multiple sclerosis.[13-16] Furthermore, ultrahigh-field MR imaging such as that at 3T might contribute to a better visualization of those tiny lesions because of a higher

Table 1. Clinical Characteristics of Subjects with CMIs

Patient No	1	2	3	4	5	6	7	8	9
Clinical diagnosis	AD	Familial AD	ICH (CAA)	VaD	AD	AD	AD	AD + CVD	DLB
Age/gender	77/F	41/F	86/F	78/M	81/F	71/F	73/M	68/M	85/M
MMSE	25	17	29	21	21	20	15	15	ND
HTN	(+)	(+)	(+)	(+)	(+)	(+)	(+)	(+)	(-)
DM	(-)	(-)	(-)	(-)	(-)	(-)	(+)	(-)	(-)
Dyslipidemia	(-)	(-)	(-)	(+)	(+)	(-)	(+)	(+)	(-)
Smoking	(-)	(+)	(-)	(-)	(-)	(-)	(+)	(-)	(-)
MRI findings									
CMBs distribution	F, T, O	F, T, P, O	P, O	F, T, P, O	F, P, O	F, O	F, P, O	F, T, P, O	F, T, O
SS	(-)	(-)	(+)	(+)	(-)	(-)	(+)	(-)	(-)
CMIs distribution	I, T	I, F, O	I, O	O, P	I, F	P	O, P	F	I, F, T
CMIs number	5	5	2	3	3	1	5	1	4
CMIs diameter (mm)	1.76-3.36	2.41-4.03	2.91-3.57	3.47-3.85	1.67-2.42	1.87	1.67-3.17	2.79	2.19-3.38

AD = Alzheimer disease; ICH = intracerebral hemorrhage; CAA = cerebral amyloid angiopathy; CVD = cerebrovascular disease; DLB = dementia with Lewy bodies; MMSE = mini mental state examination; ND = not done; HTN = hypertension; DM = diabetes mellitus; CMBs = cerebral microbleeds; SS = superficial siderosis; CMIs = cortical microinfarcts; F = frontal lobe; T = temporal lobe; P = parietal lobe; O = occipital lobe; I = insular cortex.

signal-to-noise ratio.[13-16] Therefore, in this study, we aimed to detect CMIs in vivo using these sequences on an ultrahigh-field MR scanner.

Patients and Methods

We performed a prospective analysis of 70 cognitively compromised subjects (43 female, mean age 75.3 ± 7.9 years) including AD ($n = 47$), mild cognitive impairment (MCI; $n = 14$), AD with cerebrovascular disease (CVD; $n = 3$), vascular dementia (VaD; $n = 2$), CAA-associated intracerebral hemorrhage (ICH; $n = 2$) and one each of normal pressure hydrocephalus and dementia with Lewy bodies (DLB). Their mini mental state examination (MMSE) score was 20.6 ± 4.2 (mean ± SD). All patients were recruited from the Department of Neurology, Mie University Hospital between August 2009 and August 2011. Clinical diagnosis of AD, MCI, or VaD was made by the diagnostic criteria of the DSM-IV,[17] Petersen clinical criteria,[18] or NINDS-AIREN,[19] respectively. Probable CAA was diagnosed by multiple hemorrhages restricted to the intracortical, or corticosubcortical regions on MRI using the Boston criteria.[20]

The MRI studies were performed with a 3T MR unit (Achieva, Philips Medical System, Best, the Netherlands) using an 8- or 32-channel phased-array head coil. We applied these new techniques, DIR and 3D-FLAIR images, to detect CMI in vivo. Axial DIR imaging was performed using two different inversion pulses. The long inversion time and the short inversion time were defined as the intervals between the 180° inversion pulse and the 90° excitation pulse, respectively, which had been optimized for human brain imaging and were provided by the vendor. Details of the 2D and 3D DIR protocol were as follows: field of view, 230 mm; matrix, 320 × 256 (512 × 512 after reconstruction; in-plane resolution, .45 mm × .45 mm); section thickness, 3 mm with no intersection gap; no parallel imaging; repetition time (ms)/echo time (ms), 15,000/28; long inversion time (ms)/short inversion time (ms), 3,400/325; number of signals acquired, two; and acquisition time, 4 min 30 s for 2D, field of view, 250 mm; matrix, 208 × 163 (256 × 256 after reconstruction; in-plane resolution, .98 mm × .98 mm); section thickness, .65 mm with overcontiguous slice; TSE factor 173; repetition time (ms)/echo time (ms), 5,500/247; long inversion time (ms)/short inversion time (ms), 2,550/450; number of signals acquired, two; and acquisition time, 5 min 13 s for 3D.

3D FLAIR imaging was obtained in a sagittal direction, and then the axial and coronal images were reconstructed. The details of 3D FLAIR were as follows: field of view, 260 mm; matrix, 288 × 288 (364 × 364 after reconstruction; in-plane resolution, .68 × .67 mm); section thickness, 1 mm with .5 mm overlap; no parallel imaging; repetition time (ms)/echo time (ms), 6,000/400; inversion time, 2,000 ms; number of signals acquired, two; and acquisition time, 5 min 12 s.

It is sometimes difficult to judge whether lesions are juxtacortical, mixed white and gray matters, or intracortical, because the exact anatomic border between the cerebral cortex and white matter is unclear on 3D FLAIR imaging. On the other hand, DIR shows superior delineation of gray matter, yielding an advantage over FLAIR sequence in view of greater contrast between gray and white matters, but vessels or cerebrospinal fluid pulsation artifacts are more pronounced on DIR than on FLAIR.[21] Particularly, 3D FLAIR is free from artifacts. Therefore, intracortical lesions were determined as positive if they were exclusively detected as high signal foci both on DIR and 3D FLAIR images.

Other sequences included SWI to detect CMB. The details of SWI were follows: field of view, 230 mm; matrix, 320 × 251 (512 × 512 after reconstruction; in-plane resolution, .45 mm × .45 mm); section thickness, .5 mm with overcontiguous slice; repetition time (ms)/echo time (ms), 22/11.5 (in-phase), 33 (shifted); number of signals acquired, one; flip angle 20° and acquisition time, 5 min 45 s.

The study was approved by the ethical review board of the Mie University Hospital and the subjects gave informed consent.

Results

Demographic and MRI findings of the 9 patients were summarized in Table 1. Representative MR images were presented from an AD patient with presenilin1 mutation (Fig 1 and its

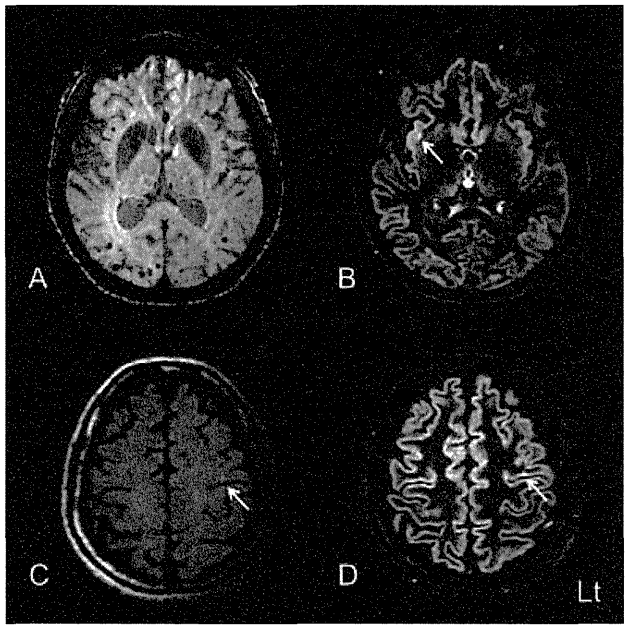

Fig 1. Head MR images in a 41-year-old woman with familial AD (Patient 2). SWI shows multiple lobar CMBs (A). DIR (B, D) and 3D-FLAIR (C) images show small intracortical hyperintense foci in the insular cortex and the left frontal lobe. Arrows indicate intracortical hyperintense foci (B, C, D).

higher magnification in Fig 2) and a patient with VaD (Fig 3). Of 70 patients, 9 (12.8%) showed intracortical hyperintense lesions, which were 2-3 mm in diameter, both on DIR and 3D FLAIR images, more obviously on the former images. The 9 patients with intracortical hyperintense lesions included 5 with AD and each 1 with AD with CVD, ICH, VaD, and DLB.

On the other hand, 38 patients (54.3%) exhibited CMBs on SWI, of which 19 (27.1%) showed multiple (≥8) lobar CMBs.[22] All the 9 patients with intracortical hyperintense lesions invariably had multiple lobar CMBs. That is, 47.4% of the patients with multiple lobar CMBs showed CMIs. These lesions were located in close proximity to CMBs (Figs 2 and 3). In a patient with AD, CMIs apparently increased in number without any significant changes of cognitive function during 1-year follow-up (Fig 4). Furthermore, 3 of the 9 patients showed local superficial siderosis adjacent to CMBs on SWI. On the contrary, those without multiple lobar CMBs showed no focal superficial siderosis or intracortical hyperintense lesions. The overlapping relationship between the subjects with CMBs, CMIs and local superficial siderosis was illustrated in Figure 5.

Discussion

In this study, we revealed multiple small intracortical hyperintense lesions in 9 patients with cognitive impairment on ultrahigh-field MRI using DIR and 3D-FLAIR images, which had been recently used to detect intracortical lesions.[13-16] These intracortical hyperintense lesions frequently adjoined lobar CMBs, and were found exclusively in subjects with multiple lobar CMBs. Lobar CMBs have been thought to indicate CAA in vivo,[23,24] and therefore, there is a strong indication that these

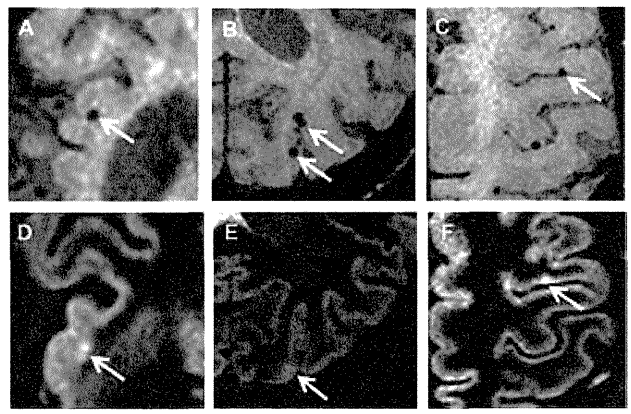

Fig 2. Higher magnification of head MR images in a 41-year-old woman with familial AD (Patient 2). Spatial close association is shown between intracortical high signal lesions on DIR (D, E, F) and lobar CMBs (A, B, C).

intracortical hyperintense lesions represent CMIs, which have a similar distribution in autopsy specimens.[1-5]

CMIs are defined as small foci confined to the cerebral cortex on histological examination.[1-6] The size of CMIs is variable. Although Haglund and colleagues[6] defined CMIs <5 mm in their paper, other studies revealed size of CMIs ranging several hundreds micrometer[1,5] and <2 mm.[4] Therefore, in this study, relatively large CMIs seemed to be detected on ultrahigh-field MRI.

The pathogenesis and disease specificity of CMIs remain unclear, however, they are a strong risk for cognitive impairment and dementia. In later life, CAA is thought to be an underlying cause for CMI. Suter and colleagues reported that CMIs were much more frequent in pathologically proven AD (32.4%) than in controls (2.5%), and that the rate increases up to 60% in the brains with AD and CAA.[4] In our pathological study, CMIs were far more numerous in AD as compared with subcortical vascular dementia, and spatially distributed very close

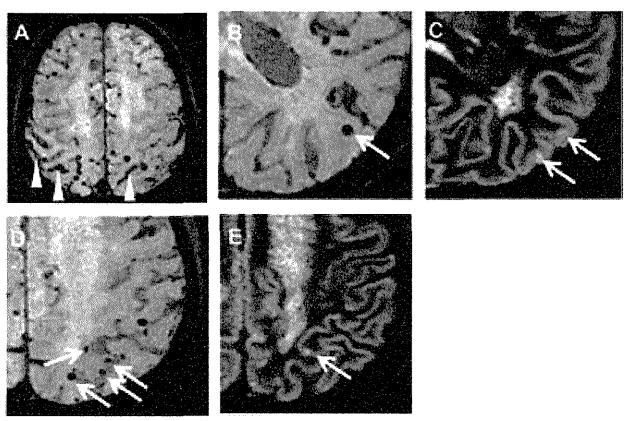

Fig 3. Head MR images in a 78-year-old man with VaD (Patient 4). SWI demonstrates multiple lobar CMBs predominantly in the parietooccipital lobes as well as focal superficial siderosis (arrowheads) adjacent to the CMBs in the bilateral parietal lobes (A). DIR image shows small intracortical high signal lesions (arrows in C, E) close to lobar CMBs (arrows in B, D).

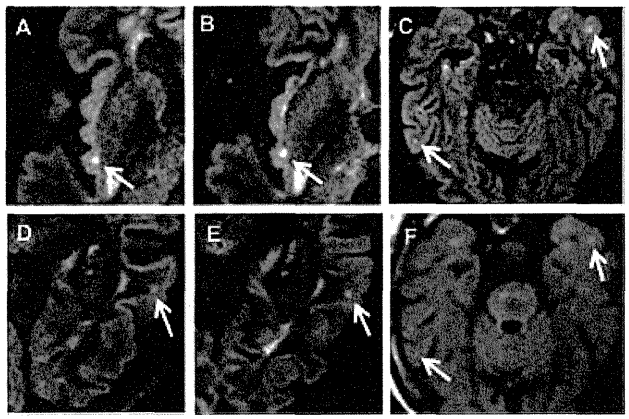

Fig 4. Head MR images in a 77-year-old woman with sporadic AD (Patient 1). DIR image shows small high signal foci in the right insula and left temporal cortices (arrows in A, D). One year later, these lesions still remained (arrows in B, E) and additional lesions appeared in the bilateral temporal lobes (arrows in C, F).

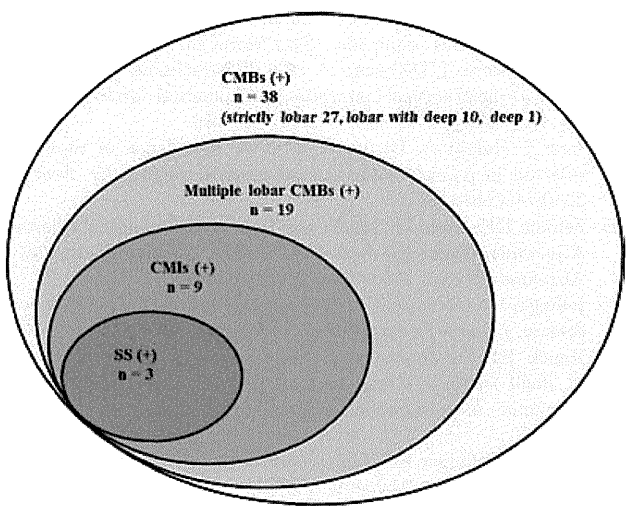

Fig 5. The relationship between the subjects with lobar CMBs, CMIs and local SS. CMBs = cerebral microbleeds; CMIs = cortical microinfarcts; SS = superficial siderosis.

to Aβ-laden small vessels with severe morphological changes.[5] Amyloid deposition affects the arterial walls, particularly of the media, of the small leptomeningeal and intracortical arteries. These vascular changes may cause chronic cerebral hypoperfusion and BBB dysfunction, and thereby result in CMIs.

According to the Boston criteria, probable CAA could be clinically diagnosed by multiple hemorrhages restricted to lobar, cortical, or cortico–subcortical regions on CT or MRI even without pathological examination.[20] In clinical practice, gradient echo T2*-weighted imaging and SWI on MRI are suitable for detecting CMBs, with apparently better sensitivity with SWI than gradient echo T2*-weighted imaging.[25,26] Lobar CMBs with a posterior predilection are frequently observed in AD patients with CAA.[10,27-30] Indeed, more than 80% of AD cases have CAA,[7] and in concert with these findings, AD patients have lobar CMBs more frequently (20-30%) than control subjects (10%).[10,22] Local superficial siderosis in the elderly, which is defined as linear low signal on T2*-weighted imaging or SWI, has been described as a late consequence of CAA-associated cortical subarachnoid hemorrhage.[31-35] Therefore, diagnostic sensitivity for CAA in the Boston criteria might be enhanced by local superficial siderosis.[20,34]

In our study, all the 9 patients with intracortical hyperintense lesions had multiple lobar CMBs with a posterior predilection, and 3 of them presented with local superficial siderosis. Particularly, one patient with DLB had multiple lobar CMBs and intracortical hyperintense lesion without risk factors of cerebrovascular disease. Recent studies suggest an association of CAA with cognitive decline in DLB in cases with concomitant AD pathology.[36,37] Therefore, all of these patients were suggested to have severe CAA, and possibly concomitant AD pathology. However, it remains elusive whether there is a straightforward correlation between the severity of CAA and AD pathology, because CAA seems to be an independent risk for dementia,[6] and unique forms of CAA (capillary CAA and pericapillary Aβ-deposits) may be readily linked to AD pathology.[38-40]

Limitations of this study include a relatively small number of subjects and lack of a clinicopathological correlation. However, a recent study had shown that intracortical infarcts have been detected in ex vivo examination of a brain with cerebral autosomal-dominant arteriopathy with subcortical infarcts and leukoencephalopathy (CADASIL) by 7-T MRI, and had discussed that these results further support the importance of cortical lesions that are not visualized on conventional MRI in small vessel disease.[41] In a clinical setting, it is important to evaluate CMIs during life, because CMIs are strong predictor for progression and severity of cognitive decline.[2,3,42,43] Apparently, further studies are required to directly compare MRI findings with pathological specimens in the near future, and prospective studies may determine the predictive value of CMIs in cognitive impairment.

In conclusion, the MRI application presented here made feasible in vivo detection of CMIs. This could be a powerful biomarker for CAA in combination with multiple lobar CMBs and focal superficial siderosis, and may further indicate vulnerability of the cerebral blood flow and the perturbed vascular network in the cerebral cortex.[42]

We thank Prof. Hidenao Fukuyama (Human Brain Research Center, Kyoto University) for his useful comment and discussion for this project.

References

1. White L, Petrovitch H, Hardman J, et al. Cerebrovascular pathology and dementia in autopsied Honolulu-Asia Aging Study participants. *Ann NY Acad Sci* 2002;977:9-23.
2. Kövari E, Gold G, Herrmann FR, et al. Cortical microinfarcts and demyelination significantly affect cognition in brain aging. *Stroke* 2004;35:410-414.
3. Kövari E, Gold G, Herrmann FR, et al. Cortical microinfarcts and demyelination affect cognition in cases at high risk for dementia. *Neurology* 2007;68:927-931.
4. Suter OC, Sunthom T, Kraftsik R, et al. Cerebral hypoperfusion generates cortical watershed microinfarcts in Alzheimer disease. *Stroke* 2002;33:1986-1992.

5. Okamoto Y, Ihara M, Fujita Y, et al. Cortical microinfarcts in Alzheimer's disease and subcortical vascular dementia. *NeuroReport* 2009;20:990-996.
6. Haglund M, Passant U, Sjöbeck M, et al. Cerebral amyloid angiopathy and cortical microinfarcts as putative substrates of vascular dementia. *Int J Geriatr Psychiatry* 2006;21:681-687.
7. Jellinger KA. Alzheimer disease and cerebrovascular pathology: an update. *J Neural Transm* 2002;109:813-836.
8. Pfeifer LA, White LR, Ross GW, et al. Cerebral amyloid angiopathy and cognitive function: the HAAS autopsy study. *Neurology* 2002;58:1629-1634.
9. Fisher M, French S, Ji P, Kim RC. Cerebral microbleeds in the elderly. A pathological analysis. *Stroke* 2010;41:2782-2785.
10. Pettersen JA, Sathiyamoorthy G, Gao FQ, et al. Microbleed topography, leukoaraiosis, and cognition in probable Alzheimer disease from the Sunnybrook Dementia Study. *Arch Neurol* 2008;65: 790-795.
11. Schrag M, McAuley G, Pomakian J, et al. Correlation of hypointensities in susceptibility-weighted images to tissue histology in dementia patients with cerebral amyloid angiopathy: a postmortem MRI study. *Acta Neuropathol* 2010;119:291-302.
12. Gouw AA, Seewann A, van der Flier WM, et al. Heterogeneity of small vessel disease: a systematic review of MRI and histopathology correlations. *J Neurol Neurosurg Psychiatry* 2011;82:126-135.
13. Wattjes MP, Lutterbey GG, Gieseke J, et al. Double inversion recovery brain imaging at 3T: diagnostic value in the detection of multiple sclerosis lesions. *AJNR Am J Neuroradiol* 2007;28: 54-59.
14. Geurts JJG, Blezer ELA, Vrenken H, et al. Dose high-field MR imaging improve cortical lesion detection in multiple sclerosis? *J Neurol* 2008;255:183-191.
15. Tallantyre EC, Morgan PS, Dixon JE, et al. 3 Tesla and 7 Tesla MRI of multiple sclerosis cortical lesions. *J Magn Reson Imaging* 2010;32:971-977.
16. Simon B, Schmidt S, Lukas C, et al. Improved in vivo detection of cortical lesions in multiple sclerosis using double inversion recovery MR imaging at 3 Tesla. *Eur Radiol* 2010;20:1675-1683.
17. American Psychiatric Association. Diagnostic and Statistical Manual of Mental Disorders-IV. Washington, DC: Author; 1994
18. Petersen RC, Doody R, Kurz A, et al. Current concept in mild cognitive impairment. *Arch Neurol* 2001;58:1085-1992.
19. Román GC, Tatemichi TK, Erkinjuntti T, et al. Vascular dementia: diagnostic criteria for research studies. Report of the NINDS-AIREN International Workshop. *Neurology* 1993;43:250-260.
20. Knudsen KA, Rosand J, Karluk D, et al. Clinical diagnosis of cerebral amyloid angiopathy: validation of the Boston criteria. *Neurology* 2001;56:537-539.
21. Turetschek K, Wunderbaldinger P, Bankier AA, et al. Double inversion recovery imaging of the brain: initial experience and comparison with fluid attenuated inversion recovery imaging. *Magn Reson Imaging* 1998;16:127-135.
22. Goos JDC, Kester MI, Barkhof F, et al. Patients with Alzheimer disease with multiple microbleeds. Relation with cerebrospinal fluid biomarkers and cognition. *Stroke* 2009;40:3455-3460.
23. Koennecke HC. Cerebral microbleeds on MRI. Prevalence, associations, and potential clinical implications. *Neurology* 2006;66:165-171.
24. van Rooden S, van der Grond J, van den Boom R, et al. Descriptive analysis of the Boston criteria applied to a Dutch-type cerebral amyloid angiopathy population. *Stroke* 2009;40:3022-3027.
25. Haacke EM, DelProposto ZS, Chaturvedi S, et al. Imaging cerebral amyloid angiopathy with susceptibility-weighted imaging. *AJNR Am J Neuroradiol* 2007;28:316-317.
26. Nandigam RN, Viswanathan A, Delgado P, et al. MR imaging detection of cerebral microbleeds: effect of susceptibility-weighted imaging, section thickness, and field strength. *AJNR Am J Neuroraiol* 2009;30:338-343.
27. Nakata Y, Shiga K, Yoshikawa K, et al. Subclinical brain hemorrhages in Alzheimer's disease: evaluation by magnetic resonance T2*-weighted images. *Ann N Y Acad Sci* 2002;977:169-172.
28. Nakata-Kudo Y, Mizuno T, Yamada K, et al. Microbleeds in Alzheimer disease are more related to cerebral amyloid angiopathy than cerebrovascular disease. *Dement Geriatr Cogn Disord* 2006;22:8-14.
29. Hanyu H, Tanaka K, Shimizu S, et al. Cerebral microbleeds in Alzheimer's disease. *J Neurol* 2003;250:1496-1497.
30. Cordonnier C, van der Flier WM, Sluimer JD, et al. Prevalence and severity of microbleeds in a memory clinic setting. *Neurology* 2006;66:1356-1360.
31. Kumar S, Goddeau, Jr. RP, Selim MH, et al. Atraumatic convexal subarachnoid hemorrhage. Clinical presentation, imaging patterns, and etiologies. *Neurology* 2010;74:893-899.
32. Raposo N, Viguier A, Cuvinciuc V, et al. Cortical subarachnoid haemorrhage in the elderly: a recurrent event probably related to cerebral amyloid angiopathy. *Eur J Neurol* 2010;18:597-603.
33. Linn J, Herms J, Dichgans M, et al. Subarachnoid hemosiderosis and superficial cortical hemosiderosis in cerebral amyloid angiopathy. *AJNR Am J Neuroradiol* 2008;29:184-186.
34. Linn J, Halpin A, Demaerel P, et al. Prevalence of superficial siderosis in patients with cerebral amyloid angiopathy. *Neurology* 2010;74:1346-1350.
35. Feldam HH, Maia LF, Mackenzie IRA, et al. Superficial siderosis. A potential diagnostic marker of cerebral amyloid angiopathy in Alzheimer disease. *Stroke* 2008;39:2894-2897.
36. Jellinger KA, Attems J. Cerebral amyloid angiopathy in Lewy body disease. *J Neural Transm* 2008;115:473-482.
37. Reuck JD, Deramecourt V, Cordonnier C, et al. Prevalence of small cerebral bleeds in patients with a neurodegenerative dementia: a neuropathological study. *J Neurol Sci* 2011;300: 63-66.
38. Attems J, Jellinger KA. Only cerebral capillary amyloid angiopathy correlates with Alzheimer pathology – a pilot study. *Acta Neuropathol* 2004;107:83-90.
39. Thal DR, Griffin WST, De Vos RAI, et al. Cerebral amyloid angiopathy and its relationship to Alzheimer's disease. *Acta Neuropathol* 2008;115:599-609.
40. Attems J, Yamaguchi H, Saido TC, et al. Capillary CAA and perivascular Aβ-deposition: Two distinct features of Alzheimer's disease pathology. *J Neurol Sci* 2010;299:155-162.
41. Jouvent E, Poupon C, Gray F, et al. Intracortical infarcts in small vessel disease: a combined 7-T postmortem MRI and neuropathological case study in cerebral autosomal-dominant arteriopathy with subcortical infarcts and leukoencephalopathy. *Stroke* 2011;42:e27-e30.
42. Miklossy J. Cerebral hypoperfusion induces cortical watershed microinfarcts which may further aggravate cognitive decline in Alzheimer's disease. *Neurol Res* 2003;25:605-610.
43. Arvanitakis Z, Leurgans SE, Barnes LL, et al. Microinfarct pathology, dementia, and cognitive systems. *Stroke* 2011;42: 722-727.

Neuropharmacology 63 (2012) 1042–1050

Contents lists available at SciVerse ScienceDirect

Neuropharmacology

journal homepage: www.elsevier.com/locate/neuropharm

Anti-amnesic effect of neurosteroid PREGS in $A\beta_{25-35}$-injected mice through σ_1 receptor- and α7nAChR-mediated neuroprotection

Rong Yang [a,b], Lei Chen [a,**], Haofei Wang [a], Bingzhong Xu [a], Hidekazu Tomimoto [c], Ling Chen [a,b,*]

[a] Department of Physiology, Nanjing Medical University, Nanjing 210029, China
[b] State Key Laboratory of Reproductive Medicine, Nanjing Medical University, Nanjing 210029, China
[c] Department of Neurology, Mie University Graduate School of Medicine, Edobashi 2-174, Tsu, Mie, Japan

ARTICLE INFO

Article history:
Received 6 April 2011
Received in revised form
16 July 2012
Accepted 19 July 2012

Keywords:
Pregnenolone sulfate (PREGS)
β-Amyloid (Aβ)
α7 nicotinic acetylcholine receptor (α7nAChR)
Sigma-1 receptor (σ_1R)

ABSTRACT

A single intracerebroventricular injection of β-amyloid 25–35 peptide ($A\beta_{25-35}$) (9 nmol/mouse) induces the spatial cognitive deterioration and approximately 50% loss of pyramidal cells in hippocampal CA1 region within 1 week. The present study focused on exploring the effects of neurosteroid pregnenolone sulfate (PREGS), in comparison with the selective agonists of sigma-1 receptor (σ_1R) and α7 nicotinic acetylcholine receptor (α7nAChR), on the cognitive deficits and the death of pyramidal cells in $A\beta_{25-35}$-mice. Herein, we reported that the administration of PREGS (1–100 mg/kg) for 7 days after $A\beta_{25-35}$-injection could dose-dependently ameliorate the cognitive deficits and attenuate the apoptosis of pyramidal cells. Either the σ_1R antagonist NE100 or the α7nAChR antagonist MLA could block the neuroprotection of PREGS in $A\beta_{25-35}$-mice. Both the σ_1R agonist PRE084 and the α7nAChR agonist DMXB could mimic the PREGS-neuroprotection against the $A\beta_{25-35}$-neurotoxicity. The neuroprotection of PRE084 was attenuated by MLA, but the DMXB-action was insensitive to NE100. The neuroprotection of PREGS, PRE084 or DMXB was blocked by the phosphatidylinositol-3-kinase (PI3K) inhibitor LY294002, whereas only the effect of PREGS or PRE084 was sensitive to the MAPK/ERK kinase (MEK) inhibitor U0126. PREGS prevented $A\beta_{25-35}$-inhibited Akt (Serine/threonine kinase) phosphorylation leading to increase in caspase-3 activity, which was σ_1R- and α7nAChR-dependent. By contrast, PREGS-rescued reduction of extracellular signal-related kinase-2 (ERK2) phosphorylation in $A\beta_{25-35}$-mice only required the activation of σ_1R. Blockage of PREGS-neuroprotection by LY294002 significantly attenuated its anti-amnesic effect in $A\beta_{25-35}$-mice. The findings indicate that the anti-amnesic effects of PREGS in $A\beta_{25-35}$-mice depend on the σ_1R- and α7nAChR-mediated neuroprotection.

1. Introduction

Alzheimer's disease (AD) is characterized by a progressive neurodegeneration leading to dementia and death. The accumulation and deposition of β-amyloid (Aβ) within the brain is thought to be the primary force driving the pathogenesis of AD. Aβ has been reported to disrupt neuronal cells by calcium dyshomeostasis (Nelson et al., 2007) and enhancement of excitotoxicity (Rothman and Olney, 1995) and apoptosis (Forloni et al., 1993). At sites of Aβ-aggregation, hippocampal neuronal cells die leading to the rapid loss of learning and memory (Yan et al., 1996).

Cholinergic system is very sensitive to the Aβ-neurotoxicity. The Aβ-induced dysfunction of α7 nicotinic acetylcholine receptor (α7nAChR) results in the impairment of spatial memory (Chen et al., 2006, 2010). The α7nAChR agonists are able to attenuate the Aβ-neurotoxicity and glutamate toxicity in cultured neurons (Kihara et al., 1997; Zamani et al., 1997). The treatment with DMXB,

Abbreviations: AD, Alzheimer's disease; Aβ, β-amyloid; DMXB, 3-(2,4-dimethoxybenzylidene)-anabaseine dihydrochloride; LY294002, 2-(4-morpholinyl)-8-phenyl-1(4H)-benzopyran-4-one hydrochloride; MLA, methyllycaconitine; MAPK, mitogenic activated protein kinase; NMDAr, N-methyl-D-aspartate receptor; NE100, N,N-dipropyl-2-[4-methoxy-3-(2-phenylethoxy)phenyl] ethylamine hydrochloride; ERK, extracellular signal-related kinase; PI3K, phosphatidylinositol-3-kinase; PREG, pregnenolone; PREGS, pregnenolone sulfate; PRE084, 2-(4-morpholinethyl)-1-phenylcyclohexanecarboxylate hydrochloride; U0126, 4-diamino-2,3-dicyano-1-4-bis [2-aminophynylthio] butadiene; α7nAChR, α7 nicotinic acetylcholine receptor; $GABA_AR$, γ-aminobutyric acid type A receptor.

* Corresponding author. Laboratory of Reproductive Medicine, Department of Physiology, Nanjing Medical University, Hanzhong Road 140, Nanjing 210029, China. Tel.: +86 25 86862878; fax: +86 25 86260332.
** Corresponding author. Tel.: +86 25 86862878; fax: +86 25 86260332.
E-mail addresses: lingchen@njmu.edu.cn (L. Chen), chenl@njmu.edu.cn (L. Chen).

0028-3908/$ – see front matter © 2012 Elsevier Ltd. All rights reserved.
http://dx.doi.org/10.1016/j.neuropharm.2012.07.035

a selective α7nAChR agonist, ameliorates the $A\beta_{25-35}$-induced deficits in spatial memory (Chen et al., 2010). Furthermore, nicotine not only inhibits beta-amyloidosis (Hellström-Lindahl et al., 2004) but also prevents the accumulation of Aβ in APP transgenic mice (Liu et al., 2007). On the other hand, the activation of sigma-1 receptor (σ_1R) may induce important neuroprotection against the $A\beta_{25-35}$-neurotoxicity (Li et al., 2010). The selective σ_1R agonists are potent neuroprotective drugs as observed in excitotoxicity models (Maurice and Lockhart, 1997; Nakazawa et al., 1998) and Aβ-induced toxicity in cortical neurons *in vitro* (Marrazzo et al., 2005). Meunier et al. (2006) have reported the potent anti-amnesic and neuroprotective effects of donepezil against $A\beta_{25-35}$-neurotoxicity through its cholinergic and σ_1R agonistic properties.

Steroids which are synthesized within the central or peripheral nervous system have been named "neurosteroids" (Baulieu, 1997). Recently, the correlation between decreased levels of neurosteroids and neuronal degeneration in AD patients has been paid close attention (Naylor et al., 2010). Pregnenolone sulfate (PREGS), a steroid synthesized de novo in the brain, is thought to relate with cognitive performance in senescent animals (Schumacher et al., 2008). Deficient cognitive performance in aged rats can be corrected by intrahippocampal injection of PREGS (Vallée et al., 1997). In addition to as a negative modulator of $GABA_A$ receptors (Akk et al., 2001) and positive allosteric modulator of N-methyl-D-aspartate receptor (NMDAr, Maurice et al., 2006), PREGS has been demonstrated to enhance the function of α7nAChR (Chen and Sokabe, 2005) and σ_1R (Monnet et al., 1995). Collectively, it is speculated that PREGS can antagonize the Aβ-neurotoxicity through its α7nAChR and σ_1R agonistic actions.

$A\beta_{1-42}$, a major constituent of senile plaques, is well known to be one of the candidates causing memory loss, because numerous studies have demonstrated a significant correlation between the number of senile plaques and the degree of cognitive deficits in AD brains. Among the Aβ fragments studied so far, peptide bearing the 11 amino acids (25–35) ($A\beta_{25-35}$) is the shortest fragment of Aβ processed *in vivo* by brain proteases (Kubo et al., 2002). This peptide retains the ability to self-aggregate and mediates the toxicity of the full-length peptide, though it lacks a hydrophobic C terminal sequence of five amino acids as compared to $A\beta_{1-40}$ (Burdick et al., 1992). It has been proposed that $A\beta_{25-35}$ represents the biologically active region of $A\beta_{1-42}$ (Pike et al., 1995). Experiments using transgenic and gene targeting mouse models have shown a close association between excess amounts of Aβ and the deficits in learning and memory. Thus, two nontransgenic rodent models of AD created by intracerebroventricular (i.c.v.) infusion of $A\beta_{1-40/42}$ (Chen et al., 2006) or $A\beta_{25-35}$ (Maurice et al., 1996) have been widely used to analyze the morphological and behavioral consequences of Aβ-neurotoxicity *in vivo*. Consistent with the $A\beta_{1-40/42}$ infusion (i.c.v.) in rats, the injection (i.c.v.) of $A\beta_{25-35}$ in mice induces, within 1 or 2 weeks after administration, histological and biochemical changes in cholinergic system (Kowall et al., 1991, 1992). A single injection (i.c.v.) of either $A\beta_{1-40/42}$ (Wu et al., 2008) or $A\beta_{25-35}$ (Chen et al., 2010) in rats and mice can impair the induction of long-term potentiation (LTP) in hippocampal CA1 region. A single injection (i.c.v.) of aggregated $A\beta_{25-35}$ (3 nmol/mouse) in mice induces amnesia in many kinds of behavior experiments such as in Y-maze, step-down type passive avoidance and Morris Water maze, although the low-dose of $A\beta_{25-35}$ does not produce neuronal cell loss (Maurice et al., 1996; Wang et al., 2007). By contrast, one single injection (i.c.v.) of $A\beta_{25-35}$ at high dose of 9 nmol/mouse can cause the death of hippocampal neuronal cells. Therefore, the present study focused on exploring the anti-amnesic and neuroprotective effects of PREGS, in comparison with the selective agonists of σ_1R and α7nAChR, after a single injection of $A\beta_{25-35}$ (9 nmol/mouse) in mice by examining the spatial memory behavioral, hippocampal morphological and biochemical changes. Our results showed that the administration of PREGS in $A\beta_{25-35}$-mice exerts a potent anti-amnesic effect through σ_1R- and α7nAChR-mediated PI3K–Akt and ERK neuroprotective mechanisms.

2. Materials and methods

2.1. Subjects

The present studies were approved by Animal Care and Ethical Committee of Nanjing Medical University. All procedures were in accordance with the guidelines of Institute for Laboratory Animal Research of the Nanjing Medical University. Male mice (ICR, Oriental Bio Service Inc., Nanjing), weighing 20–25 g (8 weeks old) at the beginning of the experiment, were used throughout the study. All animals were housed in a light controlled room under a 12-h light–dark cycle starting at AM 7:00 and kept at a temperature of 23 °C in the Animal Research Center of Nanjing University. They received food and water *ad libitum*. All efforts were made to minimize animal suffering and to reduce the number of animals used.

2.2. Preparation of an animal model of Alzheimer's disease

$A\beta_{25-35}$ (Sigma, St. Louis, MO, USA) was dissolved in distilled water at the concentration of 3 mM. "Aggregated" $A\beta_{25-35}$ was obtained by incubating at 37 °C for 4 days according to previous report (Maurice et al., 1996) and then diluted to the final concentration with saline just before the experiment. Mice were anaesthetized with intraperitoneal (i.p.) injection of chloral hydrate (400 mg/kg) and placed in a sterotactic device (Kopf Instruments, Tujunga, CA). For a single injection (i.c.v.) of $A\beta_{25-35}$, a 28-G stainless-steel needle (Plastics One, Roanoke, VA) was inserted into lateral ventricular (0.3 mm posterior, 1.0 mm lateral, and 2.5 mm ventral to bregma), and then the "aggregated" $A\beta_{25-35}$ (9 nmol/3 μl/mouse) was injected with a stepper-motorized micro-syringe (Stoelting, Wood Dale, IL, USA) at a rate of 0.5 μl/min. The injection site was confirmed in preliminary experiments by injecting Indian ink. Control mice were given an equal volume of vehicle.

2.3. Drug administration

PREGS, when intraperitoneally (i.p.) injected, may cross blood–brain barrier and can be taken up by the brain (Higashi et al., 2003). PREGS and PREG were dissolved in dimethyl sulfoxide (DMSO), and then diluted in sesame oil to a final concentration of 1.0% DMSO, because the high dose of PREGS (100 mg/kg) could not be dissolved in 1.0% DMSO diluted by saline. PREGS (1–100 mg/kg) or PREG (20 mg/kg) was subcutaneously (s.c.) injected at 100 μl once daily. σ_1R agonist PRE084 (1.0 mg/kg) and α7nAChR agonist DMXB (5 mg/kg, Taisho Pharmaceuticals, Tokushima, Japan) were dissolved by 0.9% saline and all of these drugs were intraperitoneally injected once daily on 1–7 days after $A\beta_{25-35}$-injection. NMDAr antagonist MK801 (2 mg/kg, i.p.) and σ_1R antagonist NE100 (3 mg/kg, i.p. Taisho Pharmaceutical Co. Ltd. Tokyo, Japan) were dissolved by distilled water, and α7nAChR antagonist methyllycaconitine (MLA) (0.1 nmol/mouse, i.c.v.), MAPK/ERK kinase (MEK) inhibitor U0126 (0.3 nmol/mouse, i.c.v.) and PI3K inhibitor LY294002 (0.3 nmol/mouse, i.c.v.) were dissolved in DMSO, and then in 0.9% saline to a final concentration of 1% DMSO. These antagonists were injected 30 min before treatment with PREGS or agonists. Chemicals, unless stated, all came from Sigma Chemical Company (St Louis, MO, USA). For repeated injection (i.c.v.) of drugs, a 26-G stainless-steel guide cannula (Plastics One, Roanoke, VA) was implanted into the right lateral ventricle (0.3 mm posterior to bregma, 1.0 mm lateral, and 2.3 mm ventral) and anchored to the skull with four stainless steel screws and dental cement. The drugs were prepared freshly on the day of experiment and were injected using a 28-G stainless-steel needle combining with stepper-motorized micro-syringe (Stoelting, Wood Dale, IL, USA) at a rate of 0.5 μl/min (final volume 3 μl/mouse). Control mice were given an equal volume of vehicle.

2.4. Behavioral analysis

For the Morris water maze task, a pool (diameter 90 cm) made of black-colored plastic was prepared, with water temperature maintained at 20 ± 1 °C. Swimming paths were analyzed using a computer system with a video camera (AXIS-90 Target/2, Neuroscience). In the hidden platform test, the platform (7 cm in diameter) was submerged 1 cm below the water surface. On the first and the last day of water maze training, the swimming speed was assessed in the absence of the platform. Mice were given 90 s to reach the hidden platform. Four starting positions were used and each mouse was trained with four trials per day. After reaching the platform, the mouse was allowed to remain on it for 10 s. If the mouse did not find the platform within 90 s, the trial was terminated and the animal was put on the platform for 10 s. The water maze task was consecutively performed on day 3–7 after $A\beta_{25-35}$-injection. Average swimming speed (cm/sec) and latency (sec) to reach the platform were scored on all trials and analyzed where appropriate.

2.5. Histological examination

Histological examination of hippocampal CA1 region was assessed on day 7 after $A\beta_{25-35}$-injection. Mice were anesthetized with chloral hydrate (400 mg/kg, i.p.) and perfused with ice-cold phosphate-buffered saline (PBS) followed by 4% paraformaldehyde. Brains were removed and immersed in fixative (4 °C overnight), and then processed for paraffin embedding. Coronal sections (5 μm) were cut from the level of hippocampus for toluidine blue and TUNEL staining.

In toluidine blue staining, the pyramidal cells in hippocampal CA1 region were identified using a conventional light microscope (Olympus DP70) with a 60× objective, healthy CA1 pyramidal neurons showed a round cell body with a plainly stained nucleus. Density of surviving neurons was counted in 6 sections per mouse and expressed as the number of cells per mm length along the hippocampal CA1 pyramidal layer (Cai et al., 2008).

For terminal deoxynucleotide transferase-mediated dUTP nick end labeling (TUNEL) staining, sections were deparaffinized in xylene, rehydrated through a series of graded alcohols. Subsequently, the sections were permeabilized using proteinase K (20 μg/ml) and then incubated in 3% H_2O_2 in 0.1 M PBS for 30 min in order to quench endogenous peroxidase activity. TUNEL reaction performed using In Situ Cell Death Detection Kit (Roche, Mannheim, Germany). Briefly, sections were incubated with TUNEL reaction mixture for 60 min at 37 °C. The sections were treated with Converter-POD solution and visualized by 3,3′-diaminobenzine (DAB, Chromagen Kit, Vector Laboratories) for 10 min. For positive controls, sections were incubated with DNase I for 10 min at 15–25 °C to induce DNA strand breaks, prior to labeling procedure. For negative controls, sections were incubated with label solution only (without terminal transferase) instead of TUNEL reaction mixture. The sections were observed using an Olympus (DP70) microscope with a 60× objective.

2.6. Western blot analysis

All mice were decapitated under deep anesthesia with ethyl ether on day 7 after $A\beta_{25-35}$-injection. The hippocampus was taken quickly and homogenized in a lysis buffer (50 mM Tris-HCl (pH 7.5), 150 mM NaCl, 5 mM EDTA, 10 mM NaF, 1 mM sodium orthovanadate, 1% Triton X-100, 0.5% sodium deoxycholate, 1 mM phenylmethylsulfonyl fluoride and protease inhibitor cocktail Complete; Roche, Mannheim, Germany). Total proteins (20 μg) were separated by SDS-polyacrylamide gel electrophoresis (SDS-PAGE) and transferred to a polyphorylated difluoride (PVDF) membrane. The membranes were incubated with 5% nonfat dried milk for 60 min, and then were incubated with a rabbit monoclonal anti-phosphor ERK1/2 antibody (1:1000, Cell Signaling, Beverly, MA), a rabbit monoclonal anti-phosphor Akt antibody (1:1000), or a rabbit monoclonal anti-caspase-3 antibody (1:1000) at 4 °C overnight. After being washed with TBST, the membranes were incubated with an HRP-labeled secondary antibody and developed using the ECL detection Kit (Amersham Biosciences, Piscataway, NJ). Following visualization, the blots were stripped by stripping buffer (Restore, Pierce Chemical Co, Rockford IL) for 15 min, re-blocked with 5% nonfat dried milk for 60 min, then incubated with anti-ERK1/2 antibody (1:1000), anti-Akt (1:1000) or anti-action (1:1000, Chemicon International). Western blot bands were scanned and analyzed with the image analysis software package, National Institutes of Health Image. Samples were collected from the $A\beta_{25-35}$-infused hemisphere of 3 mice as a set of western blot analysis. The summarized data represent the average of 3 experimental sets ($n = 9$ mice).

2.7. Data analysis

Data were retrieved and processed using the software Micro Origin 6.1 (Origin Lab, Northampton, MA, USA). All of data were presented as means ± standard error (SE). The significance was tested by ANOVA followed by Bonferroni's post-hoc test for multiple comparisons. Statistical analyses were performed using the Stata 7.0 software program (STATA Corporation, USA). P values less than 0.05 were accepted as statistically significant.

3. Results

3.1. PREGS improves $A\beta_{25-35}$-impaired spatial memory

The results of Morris water maze test (Fig. 1A) showed that a single injection of "aggregated" $A\beta_{25-35}$ (9 nmol/mouse) significantly increased the escape-latency to reach the hidden platform compared to control mice ($P < 0.01$ on day 5 after training, $n = 16$), whereas it did not affect the swimming speed (control: 14.71 ± 1.44 cm/s; $A\beta_{25-35}$-mice: 13.07 ± 1.63 cm/s; $P > 0.05$). The treatment with PREGS in $A\beta_{25-35}$-mice could attenuate the prolongation of escape-latency in a U-shaped dose-dependent manner ($P < 0.01$, $n = 16$; Fig. 1B). Notably, PREGS at 20 mg/kg showed the most profound effect against the $A\beta_{25-35}$-impaired

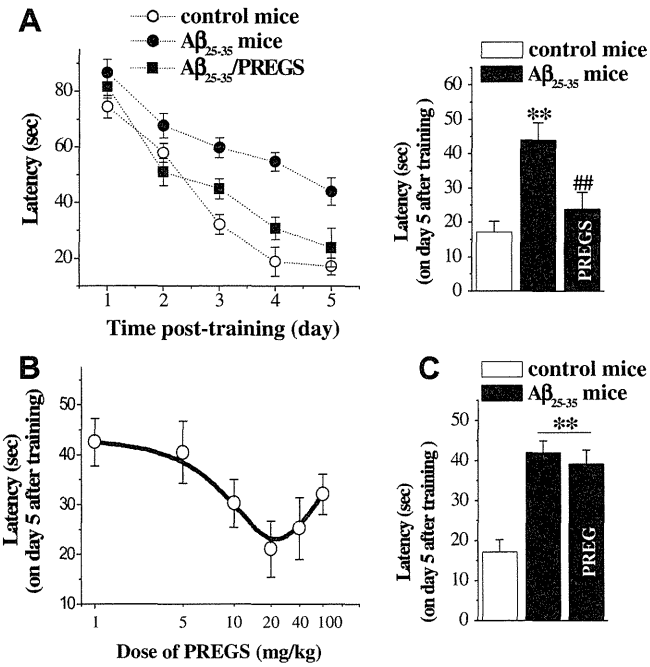

Fig. 1. Beneficial effect of PREGS on behavioral performance in $A\beta_{25-35}$-mice. (**A**) The Morris water test revealed that the latency to reach the hidden-platform was prolonged in $A\beta_{25-35}$-mice as compared with that in control mice. Treatment with PREGS (20 mg/kg) decreased the prolongation of latency in $A\beta_{25-35}$-mice. The latency was recorded from day 3 to day 7 after $A\beta_{25-35}$-injection. The histogram shows the latency on day 5 after training. (**B**) The dose-dependent curve shows the effect of PREGS (1–100 mg/kg, s.c.) on the latency in $A\beta_{25-35}$-mice. PREGS exerted the maximal effect at dose of 20 mg/kg. (**C**) Treatment with PREG (20 mg/kg) had no effect on the prolongation of latency in $A\beta_{25-35}$-mice. $^{**}P < 0.01$ *vs.* control mice, $^{\#\#}P < 0.01$ *vs.* vehicle-treated $A\beta_{25-35}$-mice.

spatial cognition, so this dose was used in the following experiments. By contrast, the administration of PREG (20 mg/kg), a non-sulfated form of PREGS, had no effect on the impairment of spatial memory in $A\beta_{25-35}$-mice ($P > 0.05$, $n = 16$; Fig. 1C).

3.2. PREGS reduces apoptosis of pyramidal cells in $A\beta_{25-35}$-mice

To explore mechanisms concerning the anti-amnesic effect of PREGS, we examined pyramidal cells in hippocampal CA1 region. The results showed that the number of pyramidal cells was reduced approximately 50% of control mice on day 7 after $A\beta_{25-35}$-injection ($P < 0.01$, $n = 8$; Fig. 2A). The treatment with PREGS in $A\beta_{25-35}$-mice markedly attenuated the loss of pyramidal cells ($P < 0.01$, $n = 8$), but PREG had no such effect ($P > 0.05$, $n = 8$). Compared with the control mice (left panel), the number of apoptotic cells (TUNEL positive cells) was significantly increased in $A\beta_{25-35}$-mice (central panel), which could be attenuated by the administration of PREGS (right panel; Fig. 2B). The results indicate that PREGS can protect neuronal cells against Aβ-neurotoxicity.

3.3. σ_1R and α7nAChR are involved in PREGS-neuroprotection

To determine the targets of PREGS-neuroprotection, we investigated the involvement of σ_1R, NMDAr and α7nAChR using the selective antagonists of the receptors. The results showed that the pre-treatment with the σ_1R antagonist NE100 almost completely blocked the neuroprotection of PREGS in $A\beta_{25-35}$-mice ($P < 0.01$, $n = 8$; Fig. 3A), while the α7nAChR antagonist MLA partially antagonized the PREGS effects ($P < 0.05$, $n = 8$). The NMDAr antagonist MK801 did not affect the neuroprotection of PREGS in $A\beta_{25-35}$-mice

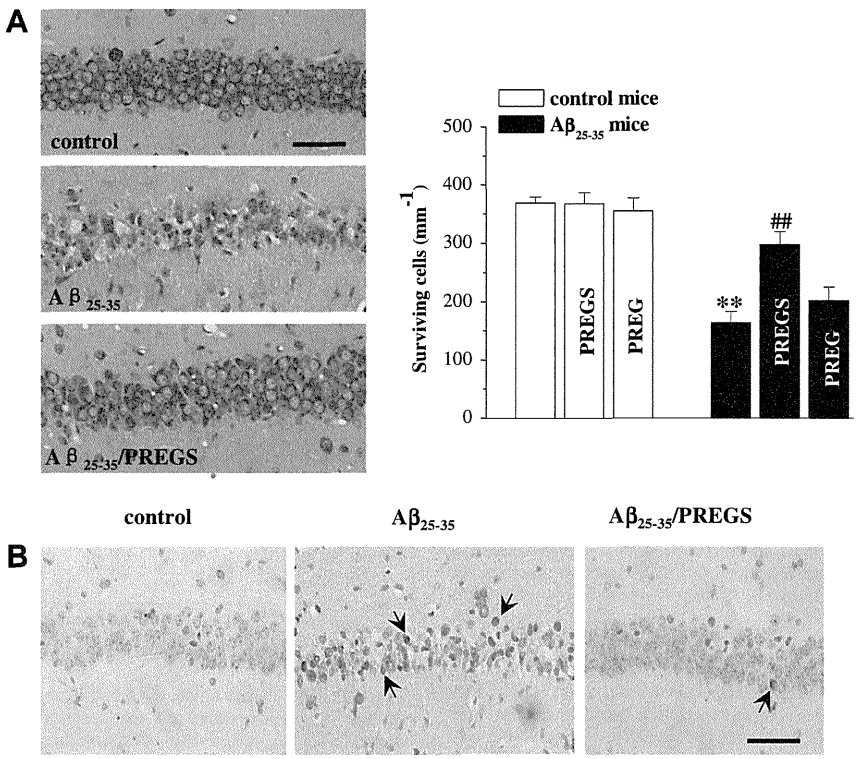

Fig. 2. Neuroprotection of PREGS on $A\beta_{25-35}$-induced neuronal death on day 7 after $A\beta_{25-35}$-injection. (**A**) Toluidine blue staining was used to evaluate the death of pyramidal cells in hippocampal CA1 region. Bar graph represents the number of surviving pyramidal cells. (**B**) TUNEL staining in hippocampal CA1 region detected the pyramidal cell apoptosis. Note that the administration of PREGS significantly reduced the apoptosis of $A\beta_{25-35}$-induced pyramidal cells. Black arrows indicate apoptosis pyramidal cells. Scale bars = 50 μM. $^{**}P < 0.01$ *vs.* control mice; $^{\#\#}P < 0.01$ *vs.* vehicle-treated $A\beta_{25-35}$-mice.

($P > 0.05$, $n = 8$), although it could reduce the death of pyramidal cells in $A\beta_{25-35}$-mice treated with vehicle ($P < 0.05$, $n = 8$).

To confirm whether σ_1R or α7nAChR is involved in the PREGS-neuroprotection, the σ_1R agonist PRE084 or the α7nAChR agonist DMXB was administered as the same protocol as the treatment with PREGS. We observed that the treatment with either PRE084 or DMXB in $A\beta_{25-35}$-mice could protect the pyramidal cells ($P < 0.01$, $n = 8$; Fig. 3B and C). Interestingly, the PRE084-neuroprotection could be blocked by MLA ($P < 0.01$, $n = 8$; Fig. 3B), whereas the DMXB-neuroprotection was insensitive to NE100 ($P > 0.05$, $n = 8$; Fig. 3C). The results indicate that PREGS targets σ_1R and α7nAChR to prevent the Aβ-neurotoxicity.

3.4. Involvement of PI3–Akt or ERK on σ_1R- and α7nAChR-mediated neuroprotection in $A\beta_{25-35}$-mice

Earlier *in vitro* study (Kihara et al., 2004) found that α7nAChR-mediated neuroprotection was related to PI3K–Akt signaling pathway rather than ERK1/2. Our results showed that in $A\beta_{25-35}$-mice, the PI3K inhibitor LY294002 could block the neuroprotection produced by PREGS, DMXB or PRE084 ($P < 0.01$, $n = 8$; Fig. 4A). By contrast, the MEK inhibitor U0126 could attenuate the neuroprotective effects of PREGS and PRE084 ($P < 0.05$, $n = 8$; Fig. 4B), but not the effect of DMXB ($P > 0.05$, $n = 8$). The administration of LY294002 or U0126 failed to affect the number of pyramidal cells in hippocampal CA1 region in control mice ($P > 0.05$, $n = 8$; Fig. 4A and B).

The phosphorylation level of Akt (p-Akt) in hippocampus of $A\beta_{25-35}$-mice was lower than that in control mice ($P < 0.05$; Fig. 5A). Treatment with PREGS could rescue the reduction of p-Akt in $A\beta_{25-35}$-mice ($P < 0.01$), which was sensitive to NE100 and MLA ($P < 0.01$). The proapoptotic protein caspase-3 activity was measured by cleavage of the caspase-3 substrate. Elevation of the hippocampal caspase-3 activity was found in $A\beta_{25-35}$-mice ($P < 0.01$; Fig. 5B). PREGS significantly attenuated the increase in caspase-3 activity in $A\beta_{25-35}$-mice ($P < 0.01$), which was also dependent on σ_1R ($P < 0.05$) and α7nAChR ($P < 0.01$). In addition, the phosphorylation level of hippocampal ERK2 (p-ERK2) was lower in $A\beta_{25-35}$-mice than that in control mice ($P < 0.05$; Fig. 5C). The treatment with PREGS in $A\beta_{25-35}$-mice could rescue the decreased level of p-ERK2 ($P < 0.01$), which was blocked by NE100 ($P < 0.01$), but not by MLA ($P > 0.05$).

3.5. Anti-amnesic effect of PREGS neuroprotection in $A\beta_{25-35}$-mice

To further explore whether the anti-amnesic effect of PREGS results from its neuroprotection, the PI3K inhibitor LY294002 was used to block the neuroprotection of PREGS in $A\beta_{25-35}$-mice (Fig. 4A). The results showed that the application of LY294002 alone did not affect the spatial cognitive performance in control mice ($P > 0.05$, $n = 16$; Fig. 6), but the treatment with LY294002 significantly attenuated the anti-amnesic effect of PREGS on the prolongation of escape-latency in $A\beta_{25-35}$-mice ($P < 0.01$, $n = 16$).

4. Discussion

One earlier study (Maurice et al., 1996) reported that the treatment with PREGS could attenuate cognitive deficits induced by a low-dose of $A\beta_{25-35}$ (3 nmol/mouse) without the loss of neuronal cells. The high dose of $A\beta_{25-35}$ (9 nmol/mouse) caused the cognitive impairment associated with the apoptosis of neuronal cells (Meunier et al., 2006). The results in the present study showed that

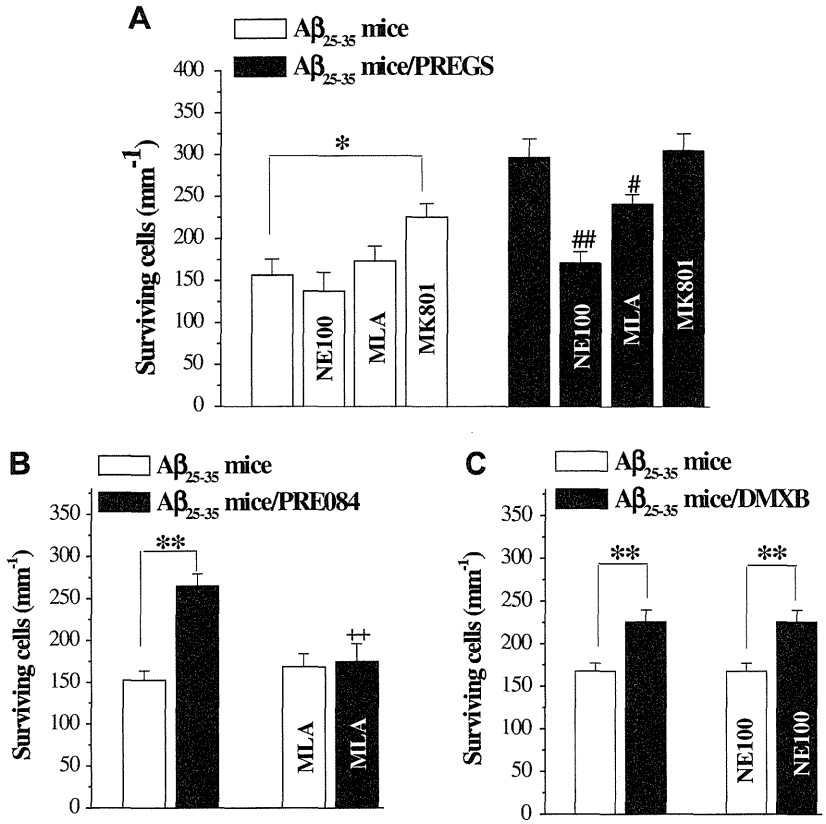

Fig. 3. α7nAChR and σ_1R are involved in the neuroprotection of PREGS in $A\beta_{25-35}$-mice. (**A**) The α7nAChR antagonist MLA, the σ_1 receptor antagonist NE100 and the NMDAr antagonist MK801 were administrated at 30 min before the treatment of PREGS. Bar graph shows the number of surviving pyramidal cells of hippocampal CA1 region in $A\beta_{25-35}$-mice. (**B** & **C**) Neuroprotective effects of the σ_1R agonist PRE084 and the α7nAChR agonist DMXB on hippocampal CA1 pyramidal cells. MLA could block the neuroprotection of PRE084, but NE100 has no effect on DMXB-neuroprotection. $^{*}P < 0.05$ and $^{**}P < 0.01$ *vs.* vehicle-treated $A\beta_{25-35}$-injected mice; $^{\#}P < 0.05$ and $^{\#\#}P < 0.01$ *vs.* PREGS-treated $A\beta_{25-35}$-mice; $^{++}P < 0.01$ *vs.* PRE084-treated $A\beta_{25-35}$-mice.

the administration of PREGS could improve the cognitive deficits and attenuate the apoptosis of neuronal cells. The neuroprotection of PREGS against Aβ-neurotoxicity depended on the activation of σ_1R- and α7nAChR to cascade the PI3K–Akt and ERK signaling pathways. Because the anti-amnesic effect of PREGS was sensitive to the PI3K inhibitor, the findings give an indication that PREGS improves the cognitive deficits in $A\beta_{25-35}$-mice through not only rescuing dysfunction of neuronal system but also protecting the neuronal cells.

4.1. Targets of PREGS-neuroprotection against $A\beta_{25-35}$ toxicity

The findings in the present study give a clear indication that the PREGS-neuroprotection against $A\beta_{25-35}$-induced apoptosis depends on the functions of σ_1R and α7nAChR. This conclusion is deduced mainly from the following observations: (1) the neuroprotection of PREGS in $A\beta_{25-35}$-mice was blocked by the antagonists of σ_1R and α7nAChR, but not the NMDAr antagonist; (2) the agonists of either σ_1R or α7nAChR could mimic the neuroprotection of PREGS to reduce the death of pyramidal cells in $A\beta_{25-35}$-mice; (3) the PREGS-effect on rescuing PI3K–Akt and ERK signals in $A\beta_{25-35}$-mice was also sensitive to the antagonist of σ_1R or α7nAChR. Because PREGS has been known to activate σ_1R (Meyer et al., 2002) and α7nAChR (Chen and Sokabe, 2005), it is indicated that PREGS directly targets σ_1R and α7nAChR, respectively. Consistent with the neuroprotective action of PRE084 in $A\beta_{25-35}$-mice, the σ_1R agonist attenuates cell death in cultured cortical neurons coincubated with $A\beta_{25-35}$, and this effect was reversed by the selective σ_1R antagonist NE100 (Marrazzo et al., 2005). Moreover, in the model of AD-type amnesia induced by low-dose of $A\beta_{25-35}$, which involves both cholinergic and glutamatergic neurotransmission through NMDAr, the σ_1R agonists and PREGS attenuate amnesia in a bell-shaped manner. Interestingly, our results showed that the σ_1R-mediated neuroprotection in $A\beta_{25-35}$-mice was blocked by the α7nAChR antagonist, while the α7nAChR-action was insensitive to the blockade of σ_1R. Thus, another possibility is that the PREGS-induced activation of σ_1R further modulates the function of α7nAChR. Detailed analysis concerning the correlation between σ_1R and α7nAChR remains to be done in the future works. One the other hand, the reduction of BDNF may be one of the major pathological conditions in AD. In hippocampus of APP/PS1 mice, the reduced BDNF could be rescued by the application of PREGS (Xu et al., 2012). BDNF activates a variety of signal molecules, including Ras/ERK and PI3K/Akt, all of which are required for survival of neuronal cells. The activation of σ_1R has been reported to selectively enhance the BDNF signaling and up-regulate the BDNF mRNA in the rat brain (Yagasaki et al., 2006). In addition, activation of σ_1 receptors facilitates neuroprotection or neuronal recovery through regulating the localization of growth factor receptors in lipid rafts (Takebayashi et al., 2004).

4.2. Possible mechanisms of PREGS neuroprotection against $A\beta_{25-35}$-toxicity

A large body of evidence emerges that $A\beta_{25-35}$ causes the necrosis of pyramidal cells in hippocampal CA1 region (Mamiya

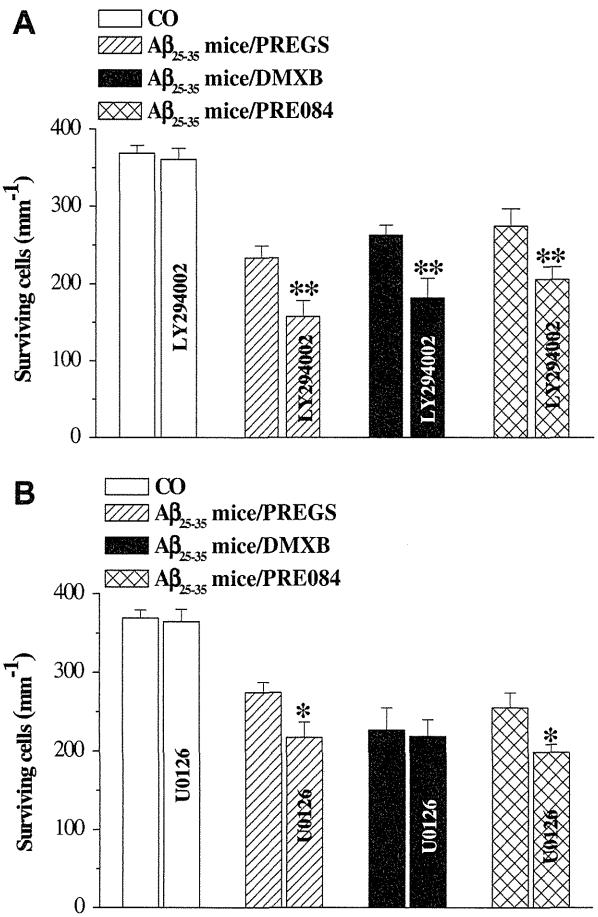

Fig. 4. PREGS-neuroprotection in $A\beta_{25-35}$-mice is *via* σ_1R- and α7nAChR-mediated ERK or PI3k–Akt signaling pathways. (**A**) PI3K inhibitor LY294002 antagonized PREGS-, PRE084- and DMXB-neuroprotection on pyramidal cells of hippocampal CA1 region in $A\beta_{25-35}$-mice. (**B**) MEK inhibitor U0126 blocked the neuroprotection of PREGS and PRE084. Neither LY294002 nor U0126 had influence on the number of pyramidal cells in control mice. $^*P < 0.05$ and $^{**}P < 0.01$ *vs.* corresponding PREGS- or agonist-treated $A\beta_{25-35}$-mice.

et al., 2004; Stepanichev et al., 2005, 2006). The $A\beta_{25-35}$-neurotoxicity in hippocampal CA1 pyramidal cells is known through down-regulating ERK and Akt phosphorylation (Daniels et al., 2001; Jin et al., 2005). Nicotinic receptor-mediated neuroprotection in the neurodegenerative disease models is related to the activation of PI3K–Akt signaling pathway (Shimohama, 2009). Several acetylcholine esterase inhibitors, including donepezil and galantamine, have been reported to attenuate the $A\beta_{25-35}$-toxicity (Arias et al., 2004; Svensson and Nordberg, 1998) through up-regulating α7nAChR-mediated PI3K–Akt signaling (Kihara et al., 2004). Our results in this study indicate that the α7nAChR agonist prevents the $A\beta_{25-35}$-downregulated PI3K–Akt signaling to reduce the caspase-3 activity. Furthermore, the activation of α7nAChR can prevent the $A\beta_{25-35}$-impaired α7nAChR (Chen et al., 2010). Consistent with the report by Kihara et al. (2004), we observed that the α7nAChR-mediated neuroprotection in $A\beta_{25-35}$-mice was independent of ERK signaling, whereas the σ_1R-mediated neuroprotection depended on the activation of ERK. Translocation of activated ERK into the nucleus (Cai et al., 2008) is necessary for the phosphorylation of cAMP response element binding protein (CREB) that elevates the expression of the pro-survival protein Bcl-2 (Meller et al., 2005). In addition, the Aβ-neurotoxicity has been shown to induce disturbance of the endocytoplasmic reticulum homeostasis and activation of stress-responsive genes, such as grp 78 or grp 94 (Yu et al., 1999; Ghribi et al., 2004). The activation of σ_1R inhibits NMDA-induced nitric oxide synthase activity to reduce nitric oxide production (Kurata et al., 2004). Hayashi and Su (2005) reported that the activation of σ_1R can inhibit the recomposition of intracellular compartments and membrane composition to prevent the $A\beta_{25-35}$-triggered mitochondrial and ER stress.

We observed that the NMDAr blocker MK801 could prevent the $A\beta_{25-35}$-neurotoxicity, suggesting that the activation of NMDAr is involved in $A\beta_{25-35}$-induced neurodegeneration. Notably, the σ_1R-dependent PREGS-neuroprotection in $A\beta_{25-35}$-mice was insensitive to the administration of MK801. Monnet et al. (1995), using the NMDA-induced [3H]norepinephrine release from rat hippocampal slices, reported that PREGS could inhibit the NMDA-response. The activation of σ_1R exerts neuroprotective effects against the ischemic injury through reducing ischemia-induced rise in $[Ca^{2+}]_i$ (Katnik et al., 2006). Kume et al. (2002) have provided supporting evidence that the σ_1R agonist reduces Ca^{2+} influx through NMDAr. On the other hand, PREGS at micromolar concentration has also been reported to directly enhance NMDA-evoked current in rat hippocampal neurons (Irwin et al., 1992; Wu et al., 1991). Thus, PREGS exerts two different effects on regulating NMDAr function: (i) a direct facilitation of NMDAr activation; (ii) an indirect σ_1R-mediated reduction of NMDA response. Although PREGS has been reported to enhance NMDA-induced excitotoxicity in cultured hippocampal neurons (Weaver et al., 2000), our results indicate that the activation of σ_1R by PREGS can inhibit NMDAr response to reduce the death of neuronal cells in $A\beta_{25-35}$-mice. Further studies are needed to evaluate whether the administration of PREGS in $A\beta_{25-35}$-mice can lead to a σ_1R-dependent decrease in the NMDA-induced Ca^{2+} influx in hippocampal CA1 pyramidal cells.

4.3. Anti-amnesic action of PREGS neuroprotection

The injection (i.c.v.) of "aggregated" $A\beta_{25-35}$ at dose of 3 or 9 nmol/mouse impairs the short-term memory in spontaneous alternation behavior, the long-term memory in step-down type passive avoidance and water-maze, although only injection of 9 nmol/mouse $A\beta_{25-35}$ causes the death of hippocampal neuronal cells (Mamiya et al., 2004; Maurice et al., 1996; Stepanichev et al., 2006). Our results in the present study showed that the administration of PREGS could exert a potent anti-amnesic effect in $A\beta_{25-35}$ (9 nmol/mouse)-mice. Blockage of PREGS-neuroprotection by the PI3K inhibitor LY294002 significantly attenuated its anti-amnesic effect in $A\beta_{25-35}$-mice, while the administration of LY294002 did not affect the spatial cognitive performance in control mice. Meunier et al. (2006) have reported the anti-amnesic and neuroprotective effects of σ_1R agonist in $A\beta_{25-35}$ (9 nmol/mouse)-mice. The results give a clear indication that the neuroprotection of PREGS against $A\beta_{25-35}$-toxicity exerts a potent anti-amnesic effect. Maurice et al. (1998) reported that the $A\beta_{25-35}$ (3 nmol/mouse)-induced deficits in alternation behavior and passive avoidance could be improved by the administration of PREGS. Wang et al. (2006) reported that the sequence 12–28 of Aβ was critical for its selective and high-affinity binding to α7nAChR. We observed that the injection of $A\beta_{25-35}$ (3 nmol/mouse) leads to the dysfunction of α7nAChR and the impairment of LTP induction (Chen et al., 2010). The treatment with the α7nAChR agonist DMXB can protect α7nAChR from $A\beta_{25-35}$-induced damage to improve the spatial cognition and the induction of LTP. Similarly, the cholinesterase inhibitor tacrine and the nicotinic receptor agonist (−)-nicotine could attenuate the $A\beta_{25-35}$ (3 nmol/mouse)-induced deficits in alternation behavior, passive avoidance and place water-maze (Maurice et al., 1996). In addition, PREGS ameliorates the $A\beta_{25-35}$ (3 nmol/mouse)-induced deficits in

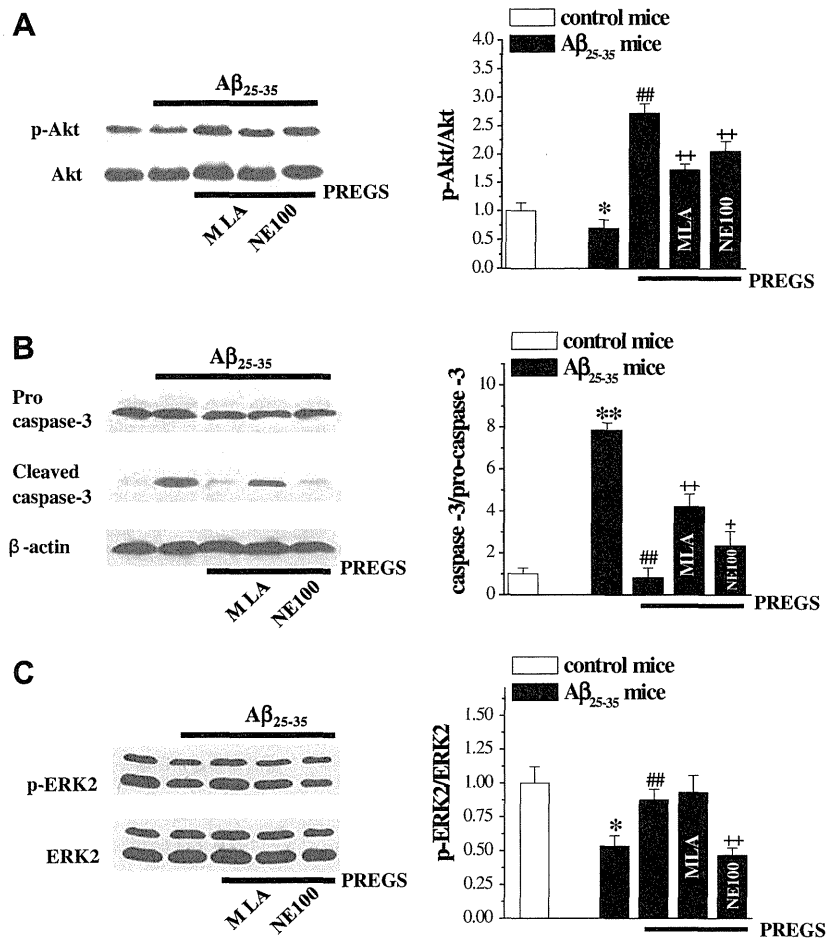

Fig. 5. PREGS prevents the $A\beta_{25-35}$-impaired Akt–caspase-3 and ERK signaling pathway in hippocampal CA1 region. (**A** & **B**) PREGS inhibited the decrease of p-Akt and the activation of caspase-3 induced by $A\beta_{25-35}$-injection, which was sensitive to NE100 and MLA. (**C**) PREGS prevented $A\beta_{25-35}$-decreased p-ERK2, which could be blocked by NE100. The densitometric values for p-Akt, caspase-3 and p-ERK2 were first normalized by the protein amounts of Akt, pro-caspase-3 and ERK2, respectively, and then were normalized again by the basal values (in control mice) of p-Akt, caspase-3 and p-ERK2, respectively. The data are expressed as the means ± SE. $^{*}P < 0.05$, $^{**}P < 0.01$ *vs.* control mice; $^{\#\#}P < 0.01$ *vs.* vehicle-treated $A\beta_{25-35}$-injected mice; $^{+}P < 0.05$, $^{++}P < 0.01$ *vs.* PREGS-treated $A\beta_{25-35}$-mice.

learning and memory, which is sensitive to the σ_1R antagonist haloperidol or BMY-14802 (Maurice et al., 1998). The σ_1R agonists are known to be potent modulators of acetylcholine release, both *in vitro* and *in vivo* (Junien et al., 1991; Kato et al., 1999). Recently, the σ_1R agonist is reported to attenuate cognitive deficits in the AD model of $A\beta_{25-35}$-injection with cholinergic loss (Antonini et al., 2011). Therefore, PREGS targets α7nAChR and σ_1R to exert the anti-amnesic effect in $A\beta_{25-35}$ (9 nmol/mouse)-mice through

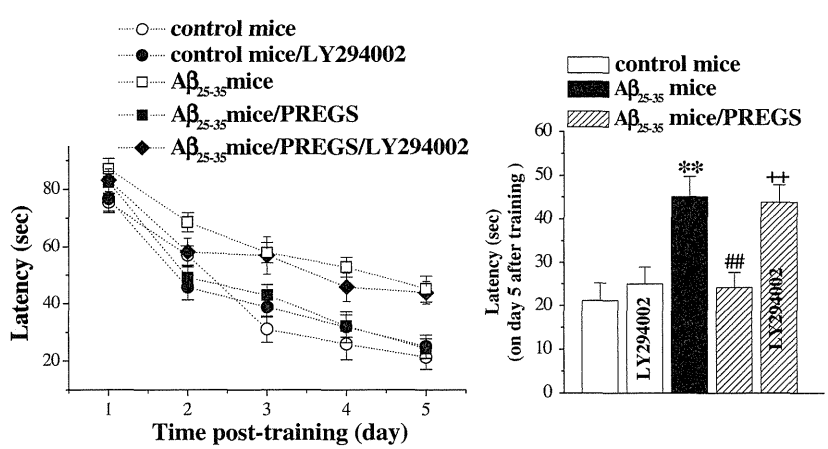

Fig. 6. Effect of PI3K inhibitor LY294002 on anti-amnesic effect of PREGS in $A\beta_{25-35}$-mice. LY294002 had no effect on the latency in control mice, but it significantly prolonged the latency $A\beta_{25-35}$-mice treated with PRGES. The latency of Morris Water maze test was recorded from day 3 to day 7 after $A\beta_{25-35}$-injection. The histogram shows the latency on day 5 after training. $^{**}P < 0.01$ *vs.* control mice, $^{\#\#}P < 0.01$ *vs.* vehicle-treated $A\beta_{25-35}$-injected mice, $^{++}P < 0.01$ *vs.* PREGS-treated $A\beta_{25-35}$-mice.